Title

- Comparative analysis of drug-salt-polymer interactions by experiment and molecular simulation improves biopharmaceutical performance

Short Title

- Analysis of drug-salt-polymer interactions

Authors

Sumit Mukesh[1]†, Goutam Mukherjee[2,3]†, Ridhima Singh[1], Nathan Steenbuck[3,4], Carolina Demidova[3,5], Prachi Joshi[1], Abhay T. Sangamwar[1*], Rebecca C. Wade[2,3,6*]

Affiliations

[1] Department of Pharmaceutics, National Institute of Pharmaceutical Education and Research (NIPER), S.A.S. Nagar, Sector-67, Punjab, 160062, India.

[2] Center for Molecular Biology (ZMBH), DKFZ-ZMBH Alliance, Heidelberg University, Im Neuenheimer Feld 282, 69120 Heidelberg, Germany

[3] Molecular and Cellular Modeling Group, Heidelberg Institute forTheoretical Studies, Schloss-Wolfsbrunnenweg 35, 69118 Heidelberg, Germany

[4] Institute of Pharmacy and Molecular Biotechnology (IPMB), Heidelberg University, Im Neuenheimer Feld 364, 69120 Heidelberg, Germany

[5] Faculty of Chemistry, Heidelberg University, Im Neuenheimer Feld 364, 69120 Heidelberg, Germany

[6] Interdisciplinary Center for Scientific Computing (IWR), Heidelberg University, Im Neuenheimer Feld 205, Heidelberg, Germany

† These authors contributed equally to this work.

*Correspondence and material requests should be addressed to A.S. (email: abhays@niper.ac.in) (experiments) or to R.C.W. (email: Rebecca.wade@h-its.org) (simulations)

Abstract

The propensity of poorly water-soluble drugs to aggregate at supersaturation impedes their bioavailability. The emergence of supersaturated amorphous drug-salt-polymer systems provides a new approach to this problem. However, the effects of polymers on drug-drug interactions in aqueous phase are largely unexplored and it is unclear how to choose an optimal salt-polymer combination for a particular drug. We describe a comparative experimental and computational characterization of amorphous solid dispersions containing the drug celecoxib, and PVP-VA or HPMCAS polymers with or without Na^+/K^+ salts. Classical models for drug-polymer interactions fail to identify the best drug-salt-polymer combination. In contrast, more stable drug-polymer interaction energies computed from molecular dynamics simulations correlate with prolonged stability of supersaturated amorphous drug-salt-polymer systems, along with better dissolution and pharmacokinetic profiles. The celecoxib-salt-PVP-VA formulations exhibit excellent biopharmaceutical performance, offering the prospect of less frequent administration and lower doses of this widely used anti-inflammatory, thereby increasing cost-effectiveness, and reducing side-effects.

Teaser

Improved pharmaceutical formulation is obtained by characterizing molecular interactions in novel drug-salt-polymer systems.

INTRODUCTION

Many pharmaceutical drugs are poorly water-soluble, and this property hinders their ability to reach the systemic circulation in the required concentration for optimal therapeutic effect. To overcome this problem, such drugs can be formulated in a high-energy amorphous solid state. This allows attainment of supersaturation exceeding the equilibrium solubility of the drug and, thereby increasing the flux across biological membranes[1-3]. However, the supersaturated state of drug molecules is metastable and there is a tendency for the drug molecules to aggregate and finally recrystallize, adversely affecting the biopharmaceutical properties of the drug[4-6]. In a typical pipeline to select excipients, such as polymers[7-9], lipids[10-12] or surfactants[13-15], to attain supersaturation of a poorly water-soluble drug (PWSD) and thereby enhance bioavailability, various supersaturated drug delivery systems are explored. A better understanding of the determinants of drug-drug and drug-excipient interactions and their relation to drug bioavailability would allow a more rational choice of drug-excipient combinations. Towards this goal, we here describe a comparative computational and experimental investigation of polymeric excipients for celecoxib (CEL) (Fig. 1A), a selective COX-2 inhibitor with a pKa of 11.1, which is a PWSD that is widely used for treating inflammatory diseases, including rheumatoid arthritis, osteoarthritis and ankylosing spondylitis,[16-18] and hence a formulation with better solubility and bioavailability would be of enormous therapeutic benefit.

The global CEL market was valued at 1149.8 million USD in 2020 and is expected to reach 1606.1 million USD by the end of 2026, growing at a CAGR (compound annual growth rate) of 8.7% during 2021-2026[19]. At present, the global CEL market is mostly dominated by Pfizer, which has formed an oligopoly marketing CELEBREX®. CELEBREX® contains micronized CEL particles, sodium croscarmellose as a disintegrant, and povidone K30 and sodium lauryl sulphate (SLS) as solubilizers, for enhancing the solubility and oral bioavailability of CEL[20]. However, SLS is an anionic surfactant that causes strong mucosal irritation and structural modification to proteins and phospholipids, leading to toxicity in humans[21-23]. Moreover, the positive food effect observed for CELEBREX® results in varying levels of absorption of CEL. Intake of CEL is recommended with food in order to improve its absorption, but due to differences in food intake, high or low fat diet, interpatient variability in the pharmacokinetic parameters can impede correct dosing [24]. Furthermore, treatment with CEL requires the administration of high doses, generally 200-400 mg twice daily for a prolonged period for treating serious conditions, which can lead to adverse events, such as hypersensitivity reactions (anaphylaxis), abdominal pain, nasopharyngitis and arthralgia, that hamper therapy[25, 26]. Thus, there is an unmet need for the development of improved dosage formulations for CEL.

We previously found that supersaturated amorphous drug-salt-polymer systems, termed amorphous salt solid dispersions (ASSD), are better than conventional binary amorphous solid dispersions (ASD) in enhancing the aqueous solubility, physical stability and bioavailability of CEL[27]. Specifically, ASSDs generated using *in situ* salt formation of CEL with Na^+ and K^+ counterions in the matrix of a Soluplus polymer exhibited the combined effects of solubility enhancement, stabilisation through ionic interactions between drug and counter-ions, and intermolecular interactions between drug and polymer, that maintain the supersaturation for prolonged times in the gastrointestinal tract

(GIT)[27]. Such prolonged effects offer the prospect of lowering the dose and for once-a-day administration that together would enhance patient compliance and reduce toxicity. These findings encouraged us to investigate in the present study whether other polymers, specifically polyvinylpyrrolidone vinyl acetate (PVP-VA) and hydroxypropyl methylcellulose acetate succinate (HPMCAS) (Fig. 1B, C), might have similar or improved effects when used with Na^+ and K^+ salts of CEL in ASSDs.

It is known that intermolecular drug-polymer interactions can significantly impact the biopharmaceutical performance[8, 9, 28] and physical stability[29, 30] of a drug. Indeed, the general rationale for experimental screening of polymers to identify excipients for a particular drug is to identify thermodynamically miscible systems that possess strong adhesive interactions (specific hydrogen bonding, hydrophobic interactions or van der Waals forces), between the drug and the polymer in order to hinder drug-drug aggregation[31, 32], and thereby prevent nucleation and crystal growth in the supersaturated solution during dissolution. The traditional methods to predict drug-polymer miscibility involve the calculation of solubility parameters and Flory-Huggins (F-H) interaction parameters[33-35]. We first applied these methods to compute solubility parameters to assess CEL-polymer miscibility for the two polymers, HPMCAS and PVP-VA. However, the results obtained from this approach did not correlate well with the measured physicochemical and biopharmaceutical attributes of the amorphous formulations of these polymers. Therefore, we took a molecular dynamics (MD) simulation approach to evaluate drug-polymer interactions.

MD simulations of drug and polymers have been employed in previous studies. For example, recent theoretical studies have employed a combination of molecular docking and MD simulations[36] or only MD simulations[37-39] to investigate molecular interactions between drug molecules and excipients. Moreover, in addition to atomistic MD simulations, coarse-grained MD simulations[40, 41] were carried out for understanding the mechanisms of inhibition of drug-drug aggregation in the presence of an excipient. Recently, Ouyang and colleagues developed machine learning methods to accelerate the development of solid dispersion formulations by aiding the selection of stable drug-polymer complexes and their evaluation by enthalpy calculations[42, 43]. However, none of these studies estimated the strength of drug-drug interactions in the presence and absence of polymer, or in the presence of ions in addition to polymer. Although molecular level mechanistic studies elucidating the drug-polymer interplay in both solution and solid state have been performed using high-end analytical techniques[6, 28, 32], the intermolecular interactions in an aqueous environment that correlate with the *in vivo* drug fate of a drug are until now largely unexplored experimentally, but are particularly amenable to investigation by MD simulation.

Here, MD simulations of CEL in neutral and anionic forms, and of CEL with different polymers, in aqueous solution, simulating the *in vivo* environment, were performed and compared with experimental measurements for novel supersaturated ASSDs that have the potential to address the aforementioned problems of drug-drug aggregation and crystallization. We find that this prevention of drug-drug aggregation is attributable to stronger drug-polymer interactions in the ionized drug state in ASSDs as compared to the non-ionized drug in conventional ASDs, thereby inhibiting the crystallisation of the drug. Of the systems studied, the simulations reveal the most stable intermolecular interactions between anionic CEL and PVP-VA, correlating with experimental observations which show prolonged stability along with ameliorated dissolution and pharmacokinetic profiles,

offering the prospect of less frequent administration and lower doses with cost-effectiveness, and therefore fewer side effects.

RESULTS

Calculation of drug-polymer miscibility parameters

The Hildebrand solubility parameter (δ) of CEL and the two polymers, PVP-VA and HPMCAS, was calculated using the Fedors and Hoftyzer-Van Krevelen (HVK) group contribution methods. The difference in the δ values of CEL and each polymer was small (<7 $MPa^{1/2}$), indicating the possibility of miscibility of CEL in these polymers (Table 1). The difference was smaller for the CEL-HPMCAS system than for the CEL-PVP-VA system (0.65 vs 1.01 $MPa^{1/2}$), indicating that the CEL-HPMCAS system should have a higher miscibility than the CEL-PVP-VA system.

Estimation of the Flory–Huggins (F-H) interaction parameter, χ, for the two CEL-polymer systems at 25ºC using the solubility parameter approach gave low positive values (Table 1). The closeness of the χ value for the CEL-HPMCAS system to zero suggests higher miscibility compared to the CEL-PVP-VA system at room temperature.

Preparation and characterization of formulations

Binary ASD formulations of CEL with PVP-VA or HPMCAS and ASSD formulations of CEL with Na^+ or K^+ and one of these two polymers were prepared using the components and following the procedure given in the Methods section and illustrated in Fig. S1. All the prepared formulations were white, free-flowing powdered solid dispersions. Optical light microscopy revealed long needle and plate shaped crystals of CEL in non-polarised mode, and showed double refraction or birefringence in polarized mode (Fig. S2A), consistent with the anisotropic crystalline nature of many drugs[44]. All the ASD and ASSD formulations presented small spherical particles in non-polarised mode and no birefringence in polarized mode (Fig. S2(B-I)) due to isotropy and the absence of a periodic crystalline lattice, revealing their amorphous nature and indicating the role of the polymers in transforming crystalline CEL to amorphous form.

These results were further supported by Differential Scanning Calorimetry (DSC) and Powder X-ray Diffraction (PXRD). In DSC, a sharp melting endotherm was observed at 163.6°C for crystalline CEL (Fig. S3a), whereas the polymer systems lacked a sharp melting endotherm and instead exhibited broad endotherms, indicating absorbed moisture. Moreover, the observation of glass transition temperature, T_g, values in the thermograms confirmed the transformation of crystalline CEL into amorphous form in the formulations (Fig. S3b-g). These T_g values range from 71.5 to 108.8 °C and are higher than the T_g of pure amorphous CEL (59.8 °C), indicating better stability of the formulations[27]. The T_g values of the ASSDs are higher than those for the ASDs, with the highest value being observed for the CEL-K-PVP-VA ASSD. The higher T_g values for ASSD formulations with PVP-VA indicate a higher heat capacity and more rigid amorphous regions, which could be due to increased ionic interactions between the drug, counterions and polymer. In PXRD, CEL showed the characteristic peak pattern of crystalline polymorphic form III

whereas a halo pattern was observed for the ASDs and ASSDs, confirming their amorphous nature (Fig. S4).

Determination of intermolecular interactions

Fourier transform infrared spectroscopy (FTIR), micro-Raman spectroscopy and nuclear magnetic resonance (NMR) spectroscopy were performed to examine the molecular level interactions between CEL, in both neutral and ionic states, and the polymers in supersaturated formulations.

FTIR spectroscopy

The overlay of FTIR spectra revealed that in the amorphous formulations, the medium intensity doublet bands, corresponding to the N–H stretching of the $–NH_2$ group, were diffused and broadened, and that the asymmetric stretching vibration of the $–SO_2$ group of CEL shifted to a lower frequency in the CEL-PVP-VA ASD and disappeared in both the CEL-PVP-VA ASSDs (Fig. 2A). This indicates the participation of the $–NH_2$ group of CEL in intermolecular hydrogen bonding with the polymer[45] and the $–SO_2$ group of CEL in salt formation with the counterion due to the greater electronegativity of the oxygen atom than the nitrogen atom, which is attributed to the -R effect (negative resonance) shown by the sulphonamide group (Fig. 1A). The interaction of CEL with the counterion can also be observed in the crystal structure of the CEL-Na^+ salt[46]. The weaker electrostatic interaction between CEL and the K^+ counterion is due to the larger ionic radius and lower charge density of K^+ as compared to the Na^+ counterion[27, 47].

The –C=O stretching frequency of the VA moiety of PVP-VA at 1667 cm^{-1} shifted downfield in the ASD and ASSDs, suggesting the formation of hydrogen bond between the –C=O group of the polymer and the –NH group of CEL. The –C=O stretching frequency of the VP moiety of PVP-VA at 1731 cm^{-1} shifted in the ASSDs but there is no change in frequency for the ASD. Moreover, the –C–F symmetric stretching vibrations peak at 1228 cm^{-1} in CEL shifted to higher frequencies in all the PVP-VA and HPMCAS formulations and its intensity reduced, confirming the formation of disordered amorphous structures[48] (Fig. 2A,B).

For the CEL-HPMCAS systems, the doublet of $–NH_2$ protons of CEL at 3337 cm^{-1} and 3232 cm^{-1} shifted and broadened in all the formulations, indicating the formation of a hydrogen bond. The –S=O peak at 1346 cm^{-1} in CEL shifted to 1345 cm^{-1}in the ASD, but dissipated in both CEL-HPMCAS ASSDs, indicating salt formation. The –C=O stretching frequency of HPMCAS at 1739 cm^{-1} shifted to 1738 cm^{-1} in the ASD and 1734 cm^{-1} in the CEL-Na-HPMCAS ASSD, but disappeared in the CEL-K-HPMCAS ASSD, suggesting hydrogen bond formation between the –C=O group of the polymer and the –NH group of CEL (Fig. 2B).

These results indicate that the counterion ($Na^{+/}K^+$) interacts with CEL via strong ionic interactions resulting in the formation of salt. Also, the *in situ* generated salt and variations in the peak shifts suggest that CEL is hydrogen-bonded to both the –C=O groups of the PVP-VA polymer. These hydrogen bonds may help maintain the supersaturation of CEL in solution for long times by inhibition of nucleation and crystal growth.

Micro-Raman spectroscopy

Previously[27], we described the characteristic peaks of CEL present in the micro-Raman spectrum range of 1000-1700 cm^{-1} and here we focused on the same range (Fig. 2C). Crystalline CEL exhibited a characteristic peak of –S=O asymmetric stretching at 1158 cm^{-1}. The disappearance of this peak in all the CEL ASSDs confirms electrostatic interactions between the CEL's –S=O group and the counterions (Na^+/K^+), resulting in salt formation. However, the -S=O peak also disappeared in the CEL-HPMCAS ASD, which cannot be due to salt formation but may be due to its hydrogen bonding interaction with the -OH group of HPMCAS. Furthermore, the –NH peak present for crystalline CEL at 1573 cm^{-1} disappeared in all the formulations, confirming the hydrogen bonding interactions between the –NH group of CEL and the –C=O of the polymer as also observed in FTIR spectra. Thus, the FTIR and micro-Raman spectroscopy both reveal *in situ* salt formation of CEL with the counterion and CEL hydrogen bonding with the polymer.

NMR spectroscopy

Chemical shifts in the aliphatic and aromatic regions of CEL as a result of alterations in the proton microenvironments were measured by NMR[32] for CEL and its amorphous formulations (Fig. S5, Fig 2D). The upfield shift in the two doublet peaks of aromatic protons attached to sulphonamide group of CEL and the disappearance of the $–NH_2$ peak at a chemical shift of 7.52 ppm in ASSDs, but not ASDs (Fig. 2D), confirmed salt formation between CEL and the counterion (Na^+/K^+) due to loss of a proton from the $–SO_2NH_2$ group, leading to shielding of the neighbouring aromatic protons in CEL. In the $–SO_2NH_2$ group, the $−NH_2$ and $−SO_2$ act as proton donor and acceptor, respectively. The $−SO_2$, being a strong electron-withdrawing group, will undergo a -R effect due to conjugation between the lone pairs of electrons of the oxygen atoms and the pi electron of the resonating system, and there is a delocalisation of pi electrons towards the oxygen atoms, which further extracts electrons from the N atom of the $–NH_2$ group and leads to formation of the -S=NH bond. This effect will lead to more electron-rich oxygen atoms that can make an ionic interaction with the positively charged counterion (Fig. 1A). Furthermore, the upfield shifts of the aromatic protons in the ASSDs indicate a change in their electron density because of the drug-polymer interactions. The doublet peaks of the aromatic protons in CEL at chemical shift values of 7.87 and 7.54 ppm were shifted upfield in the ASSDs, whereas no such alteration in the peaks was observed for the ASD formulations (Fig. 2D). Hydrophilic polymers can interact with drug molecules either by forming electrostatic interactions or by hydrogen bonding, thereby inhibiting drug-drug aggregation and maintaining supersaturation for prolonged times [27]. The CEL chemical shifts, along with the enhanced T_g obtained in the DSC studies, further confirm the *in situ* salt formation between CEL and the counterion (Na^+/K^+) and the drug-polymer interactions in the ASSD formulations.

Supersaturation and precipitation studies

The extent of CEL supersaturation in the ASSDs in comparison to the ASDs was studied at 37 °C using an ultraviolet (UV) spectrophotometer. Excess CEL was dissolved in methanol at 5 mg/mL concentration and poured into 25 mL water. Initially, a high absorbance was observed for CEL followed by a rapid decline due to precipitation of CEL in water. The CEL-K-PVP-VA ASSD generated maximum supersaturation of CEL for 4 h due to the hydrophilic nature of the PVP-VA polymer, however the CEL-Na-PVP-VA ASSD showed a slower decline in CEL concentration for 40 min and maintained it for 4 h

(Fig. S6B). This confirmed the greater prevention of water-induced crystallization of CEL in the CEL-K-PVP-VA ASSD than in the CEL-Na-PVP-VA ASSD. The CEL in the binary ASD with both the polymers showed reduced absorbance in comparison to the ASSDs due to crystallization from its supersaturated state, which can be attributed to weaker intermolecular interactions between CEL and the polymer in the neutral state than in the ionic state. The ASSDs with HPMCAS were less performant in the maintenance of supersaturation of CEL (Fig. S6A) due to the lower aqueous solubility of HPMCAS. The presence of the comparatively less hydrophilic methoxy and acetate substituents makes HPMCAS water-insoluble when unionized at about pH < 5 and it remains predominantly in a colloidal state at intestinal pH (i.e., pH 6.0–7.5). This ultimately results in poor aqueous solubility of the polymer even in its ionized state at the small intestinal pH and leads to the formation of colloidal polymer aggregates in aqueous solutions that promote interactions within the polymer[49]. The better behaviour of the systems containing PVP-VA than those containing HPMCAS was contrary to the predictions from the calculation of drug-polymer miscibility parameters (Table 1). Therefore, to investigate the physical mechanisms underlying the supersaturation of CEL in both neutral and ionic states with and without polymer, we next performed molecular modelling and simulation.

***In silico* molecular modelling.**

The systems simulated, labelled a-j, are listed in Table 2.

Refinement of polymer models by MD simulations. Explicit solvent MD simulations of the individual polymers were initiated with either a PVP-VA or a HPMCAS oligomer in a rather extended modelled conformation in a periodic box of aqueous solution (Fig. 3). The oligomers of the two polymers deviated from linearity and adopted bent structures during the simulations. The all-atom root-mean-square deviation (RMSD) values showed convergence during the simulations (Fig. S7 a and b).

Simulation of CEL aggregation. First, simulations were conducted to model the amorphous forms of CEL (both neutral and anionic forms) in the absence of polymer and the presence of ~0.01M NaCl (see Table 2 and Methods for further details). CEL aggregates during simulations in aqueous solution at supersaturated concentration. The neutral form of CEL aggregated within a few hundred ns in MD simulations in aqueous solution without any polymer (Fig. 3). On the other hand, the anionic form of CEL only partially aggregated during one simulation (system e, final snapshot at 916 ns shown in Fig. 3) and remained dissociated during the other simulation (system f simulated for 1042 ns). In the aggregates of CEL, no specific non-covalent interactions were found, except that for neutral celecoxib, an intermolecular hydrogen bonding interaction was observed between the sulfonamide $-NH_2$ group of one CEL molecule and the $-SO_2$ group of another molecule (see radial distribution function (RDF) in Fig. 4A (a)). The same interaction was much reduced for the anionic form of CEL (Fig. 4A (b)). These results support the faster aggregation of CEL in the neutral state than in the ionic state, in the absence of polymer, due to stronger interactions between the CEL molecules.

Simulation of CEL-polymer systems. Simulations were next performed for CEL in the presence of polymer and ~0.01M NaCl and the aggregation propensities of the CEL:polymer systems was compared with the CEL-CEL systems (see Table 2 and Methods for further details). The CEL-polymer interactions modulate CEL:CEL hydrogen-bonding interactions. We performed two sets of MD simulations per CEL-

polymer combination and analysed the trajectories in terms of hydrogen bond contact occupancy and RDFs, and computed interaction free energies with the MM/GBSA method.

Interactions between PVP-VA and CEL. For PVP-VA, a hydrogen bond (average occupancy among two sets ~43%) was observed between the sulfonamide $-NH_2$ group of CEL and the carbonyl (−C=O) group on the VP and VA moieties of PVP-VA which would affect the hydrogen bonding between CEL molecules. The RDF between the $-NH_2$ group of the neutral form of CEL and all oxygen atoms of the PVP-VA polymer shows a clear peak (Fig. 4B (a-b)) at 2.8±0.01 Å, whereas this peak is absent for the anionic form of CEL. In the presence of PVP-VA, the relative g(r) value of the CEL sulfonamide $-NH_2$ and $-SO_2$ groups is lower (Fig. 4A (c)) than in the absence of polymer (Fig. 4A (a)). Thus, the CEL:CEL hydrogen-bonding interactions are weakened by the presence of the PVP-VA oligomer.

Interactions between HPMCAS and CEL. The RDF was computed for each of the five individual functional groups of HPMCAS and for all the five groups together. The g(r) values between the neutral form of CEL and the hydroxypropoxy and hydroxyl groups of HPMCAS are the highest in both sets of simulations (Fig. 4B (e-f)). The g(r) at a distance ≤3 Å between the hydroxypropoxy group of HPMCAS and the anionic form CEL (Fig. 4B (g-h)) is less than for the neutral form of CEL, but much higher than the carbonyl oxygen of the VA group of PVP-VA (Fig. 4B (c-d)). As observed for PVP-VA, the relative g(r) value of sulfonamide−NH2 and −SO2 groups of CEL in the presence of HPMCAS, is also decreased (Fig. 4A (e)) in comparison to the corresponding value in the absence of polymer (Fig. 4A (a)). Thus the CEL:CEL hydrogen-bonding interactions are also weakened by the presence of the HPMCAS oligomer.

Effect of polymer on CEL aggregation. The role of a polymeric excipient is to inhibit the crystallization process of PWSDs through intermolecular interactions. Moreover, the drug-polymer complex should be stable enough in solution to prevent drug aggregation. Thus, to find an optimum polymer for a particular drug, it is necessary to check the stability of a drug-oligomer complex during MD simulations as well as to estimate the drug aggregation and drug-oligomer complexation energies.

Upon analysing the MD trajectories, we found stable CEL:oligomer complexes and a reduction in CEL:CEL interaction energy in the presence of an oligomer for the neutral form of CEL (Fig. 5 and Table S1). For the anionic form of CEL, partial or no aggregation was observed in the absence of oligomer, whereas relatively stable CEL aggregates were observed in presence of oligomers. Of the two polymers considered here, PVP-VA formed a more stable complex with the neutral and anionic forms of CEL. Interestingly, the PVP-VA oligomer formed a relatively more stable complex with the anionic than the neutral form of CEL. This is due to the higher degree of intermolecular contact between the fluorine atoms of anionic CEL and the carbonyl carbon atoms of the PVP-VA oligomer as observed in the RDF analysis between these atoms (Fig. S8). This interaction strengthened the electrostatic and van der Waals forces between the PVP-VA oligomer and the anionic form of CEL (Table S2). On the other hand, the electrostatic interaction energy between the anionic form of CEL and the HPMCAS oligomer is unfavorable due to repulsive interactions between the negatively charged sulfonamide group of CEL and the oxygen atoms of the oligomer. Nevertheless, the overall energy of the complex is negative due to the favorable van der Waals and solvation energies.

We also found that as the strength of oligomer:CEL interaction energy increased, the CEL:CEL interaction energy tended to decrease. Per celecoxib molecule, the strength of the oligomer:CEL interaction is several-fold higher than that of the CEL:CEL interaction in the aggregate for both neutral and anionic forms of CEL. From energy component analysis, we found that in the neutral form of the CEL aggregate, the intermolecular van der Waals component is more favourable than the electrostatic energy. For the anionic form of CEL in the presence of HPMCAS, the electrostatic energy term was highly unfavourable. However, due to the favourable solvation and van der Waals interaction energies, the overall binding free energy is favourable between CEL molecules in the anionic form and HPMCAS oligomer. Since the CEL:PVP-VA interactions are stronger than the CEL:HPMCAS interactions for both neutral and anionic forms of CEL, PVP-VA could serve as a candidate polymer for CEL for preventing its precipitation and maintenance of supersaturation for prolonged times due to more favourable intermolecular interactions between the drug and the polymer. Notably, the order of the MM/GBSA CEL:CEL binding free energy both in neutral and anionic forms of CEL in the absence and presence of polymer, is different from that derived from the computed solubility parameters (Table 1) but correlated with the experimentally observed intermolecular interactions and biopharmaceutical performance as measured in the next section.

Evaluation of solubility, dissolution and biopharmaceutical performance of the amorphous formulations

Apparent solubility studies. Apparent solubility studies performed in distilled water for 6 h showed different solubilities of CEL in its different formulations (Fig. 6A). Crystalline CEL attained the maximum solubility of 4.53 µg/mL after 30 minutes, whereas for the CEL-PVPVA and CEL-HPMCAS ASD formulations, the highest solubility obtained was 34.96 and 20.26 µg/mL, respectively after 5 minutes. For the CEL-Na-PVP-VA and CEL-K-PVP-VA ASSD formulations, the maximum solubility was attained within 5 minutes and was 736.87 and 392.48 µg/mL, respectively, whereas for the CEL-HPMCAS-Na and CEL-K-HPMCAS ASSD formulations, the maximum solubility obtained was 73.88 and 193.19 µg/mL after 15 and 30 minutes, respectively. However, the drug concentration declined afterwards for the ASSDs, whereas no such changes were observed for the ASD. The supersaturation was maintained for the ASSDs and the concentrations achieved after 6 hours were 139.54 and 154.72 µg/mL for CEL-Na-PVP-VA and CEL-K-PVP-VA ASSDs, respectively, and 25.54 and 126.80 µg/mL for CEL-Na-HPMCAS and CEL-K-HPMCAS ASSDs, respectively. The enhancement in solubility with respect to crystalline CEL was over 40-fold in the PVP-VA ASSD and up to 36-fold in the CEL-K-HPMCAS ASSD. The CEL embedded in the formulations is in amorphous form, as supported by DSC and XRD spectra (see Fig. S3 and S4, respectively), and dissolved immediately in the aqueous environment (spring effect) and attained supersaturation (parachute effect). The combined effect of the loss of the crystal lattice energy and the pH buffering effect of the salt in ASSD formulations accounted for the higher apparent solubility of CEL, and extended supersaturation (see Fig. S6) due to stable intermolecular interactions. This spring and parachute phenomenon is important for significant dissolution and augmented the *in vivo* bioavailability of the drug[8].

In vitro dissolution studies. *In vitro* dissolution studies were performed to understand the release behavior of pure crystalline CEL and, CEL from amorphous ASD and ASSD formulations under sink and non-sink conditions.

Dissolution under sink conditions. The dissolution studies were performed at pH 12 using tribasic sodium phosphate buffer (1000 mL media) as recommended by the Office of Generic Drugs (OGD), USFDA. As per United State Pharmacopoeia (USP), the sink condition is defined as the condition in which one entire dose of the drug is solubilized in one third of the volume of the dissolution medium. The equilibrium solubility of pure crystalline CEL in pH 12 dissolution medium was found to be around 569.80 µg/mL. Accordingly, the entire 100 mg dose of the CEL would solubilize in 175 mL of the dissolution volume.

Crystalline CEL showed release of 18.73 % after 120 min whereas the formulated binary CEL-PVP-VA and CEL-HPMCAS ASD exhibited CEL release of 88.00 % and 82.17%, respectively, after 120 min. For CEL-Na-PVP-VA ASSD, 100.00 % of CEL was released within the initial 10 min. However, the released CEL concentration declined to 97.55 % due to its de-supersaturation after 120 min. CEL-K-PVP-VA ASSD manifested a CEL release of 98.46 %. In CEL-Na-HPMCAS ASSD, a rapid increase in the CEL release was observed in the initial 5 min followed by supersaturation maintenance over a period of 120 min with a CEL release of 89.27 %. In contrast, CEL-K-HPMCAS ASSD showed a gradual increase in CEL release, reaching 95.67 % after 120 min, slightly higher than for CEL-Na-HPMCAS ASSD (Fig. 6B).

The ASD and ASSD formulations followed the concept of spring and parachute effects. CEL was released rapidly above the saturation level due to its amorphous nature in the formulations (spring effect), and the supersaturation was further maintained because of the presence of polymer in close proximity with drug that avoids solution-induced crystallization through strong drug-polymer interactions (parachute effect). For the ASSD formulations, CEL solubility was enhanced due to salt formation, and the dissolution performance was better than for the corresponding binary ASD, thereby achieving improved bioavailability. The increment in dissolution rate is attributable to the dual benefit of ASSD i.e., amorphization and salt formation, due to the loss of crystal lattice energy and self-buffering capacity, respectively. The dissolution rate is dependent on the release of drug from the diffusional double layer around the dissolving particle in the medium. The salt alters the pH of the microenvironment around the dissolving drug particle and promotes its ionization, and faster dissolution as compared to free acid or base[50].

Dissolution under non-sink conditions. This set of dissolution studies was performed in pH 11 tribasic sodium phosphate buffer. The equilibrium solubility of CEL in this buffer was found to be 28.09 µg/mL. Therefore, the entire 100 mg dose of the CEL cannot be solubilized in one third of the volume of the dissolution medium and the system corresponds to non-sink conditions and provides a more realistic estimate of the ability of amorphous solid based formulations to increase the release of PWSD in the GIT. Crystalline CEL showed a low release rate of 6.96 % in pH 11 buffer after 120 min because of its low solubility and poor wetting behavior. Because of its hydrophobic nature, CEL tended to float on the surface of the dissolution medium during the study period. The CEL release exhibited by the CEL-PVP-VA ASD was approximately 70.62 % after 120 mins, which was considerably lower than for the PVP-VA ASD. On the other hand, the CEL release of the CEL-HPMCAS binary ASD was higher at 81.32 % compared to that for the CEL-Na-HPMCAS and CEL-K-HPMCAS ASSD for which the CEL release was 78.53 % and 68.08 %, respectively after 120 minutes (Fig. 6B), indicating slow and incomplete release from the HPMCAS polymeric matrix. However,

469 both the CEL ASSD formulations displayed approximately 12-fold enhancement in the
470 percentage of drug release compared to pure crystalline CEL.

471 CEL-Na-PVP-VA and CEL-K-PVP-VA ASSD formulations exhibited a similar pattern of
472 maximum drug release, with 85.09 % and 85.98 % release after 120 mins (Fig. 6B).
473 Moreover, a difference of approximately 40.00 % was observed in the release profiles of
474 CEL-PVP-VA ASD and its ASSD for the initial 10 min, with the difference falling to
475 15.00 % after 120 min. Apart from strong ionic interactions in amorphous salts, strong
476 CEL-polymer interactions in both the ASSD prevented the aggregation of CEL particles
477 from the supersaturated solution. Under non-sink conditions, the ASSD prepared with the
478 HPMCAS polymer did not generate supersaturation greater than its binary ASD. The CEL
479 release from both the ASSD was gradual and ASSD prepared using PVP-VA exhibited
480 better drug release than HPMCAS because of the formation of pores in the PVP-VA
481 matrix during dissolution. The greater the amount of PVP-VA the higher will be the pore
482 size, which would further effect the dissolution[51]. The higher dissolution of ASSD
483 formulations corresponded to their *in vivo* biopharmaceutical performance.

484 ***In vivo pharmacokinetic studies.*** The *in vivo* performance of the amorphous formulations
485 was further assessed by pharmacokinetic studies. Crystalline CEL showed a maximum
486 plasma concentration (C_{max}) of 21 ng/mL at 1 h whereas CEL-PVP-VA and CEL-
487 HPMCAS binary ASD showed C_{max} of 56 ng/mL (at 2 h) and 52 ng/mL (at 1 h),
488 respectively. The CEL-K-PVP-VA and CEL-Na-PVP-VA ASSD exhibited higher C_{max}
489 values of 167 ng/mL and 116 ng/mL, respectively, at 12 h whereas the CEL-Na-HPMCAS
490 ASSD attained a C_{max} of 84 ng/mL at 1 h, which further reduced with time. Also, CEL-K-
491 HPMCAS ASSD acquired a lower C_{max} of 60 ng/mL, even at 12 h (Fig. 6C). Thus, CEL-
492 K-PVP-VA and CEL-Na-PVP-VA ASSD had approximately 8.0 and 5.6-fold higher C_{max},
493 respectively, than crystalline CEL. Moreover, the extent of enhancement in C_{max} and other
494 pharmacokinetic parameters was much greater for the ASSD than the binary ASD, see
495 Table 3. Both the ASSD formulations of CEL with PVP-VA possessed a higher plasma
496 concentration of CEL for 12 h due to maintenance of supersaturation for a prolonged
497 period (synergistic effect of amorphization and salt form), enhanced solubility and
498 dissolution, and increased intermolecular drug-polymer interactions in the ionic state than
499 in the neutral state, thereby inhibiting drug-drug aggregation as revealed from the
500 experimental and *in silico* computational interaction studies. This may be ascribed to
501 generation of CEL-rich nano-droplets or a colloidal system in equilibrium with the
502 molecularly dissolved CEL[52]. Also, the PVP-VA matrix allowed higher CEL loading,
503 and enabled carrier-controlled release for continuous dissolution of CEL through gel-like
504 layer of PVP-VA, and absorption into the blood stream gradually over a longer time
505 period[51]. However, the binary ASD showed lower supersaturation potential then the
506 ASSD due to weak intermolecular interactions between CEL and PVP-VA, resulting in a
507 lower C_{max} (56 ng/mL). Additionally, the formulations with HPMCAS did not prove better
508 than PVP-VA, indicating the lower supersaturation potential of HPMCAS that is evident
509 from its lower solubility at lower pH (10% below pH 4 and 50% at pH 5). Notably, the
510 solid dispersion of paclitaxel (PTX) with HPMCAS-MF failed to improve the oral
511 bioavailability of PTX in Sprague Dawley (SD) rats despite maintenance of *in vitro*
512 supersaturation[53].

513 **Stability Studies.** The physical stability of the ASSDs was evaluated at ambient
514 conditions and compared to that of the corresponding binary ASDs. All the ASSD
515 formulations were found to be stable for more than 11 months (352 days) at the ambient

temperature and relative humidity present in the lab. Even after 11 months storage, DSC thermograms of ASSD formulations prepared with Na^+ or K^+ counterions showed no recrystallization and no melting endotherm (see Fig. S10). The DSC thermograms correlated well with the optical and polarised light microscopy data which showed no birefringence in polarised mode (see Fig. S11). The results support the amorphous nature of the formulations and the absence of recrystallization, indicating the prolonged physical stability of ASSD formulations. ASDs, on the other hand, showed a melting endotherm in DSC thermograms after 11 months, suggesting recrystallization occurred and indicating poor physical stability (see Fig. S10). Consistently, in optical and polarized light microscopy images, birefringence was observed in the polarized mode, confirming the presence of crystallinity in the samples and the loss of the amorphous nature (see Fig. S11). Hydrogen bonds in the ASDs were not able to prevent crystallization over longer time periods whereas the stronger ionic interactions in the ASSDs could. Thus, the ASSD formulation enhanced the physical stability of the amorphous form over long times in comparison to conventional ASDs.

Scanning electron microscopy (SEM). The surface morphology was observed for the ASD and ASSD formulations using SEM (see Fig. S12). The CEL-Na-PVP-VA ASSD revealed a mixture of spherically shaped smaller and larger particles, with curved surfaces inside the core. This may be due to the drying of particles from the surface during spray drying process. On the other hand, the CEL-PVP-VA ASD showed spherical particles with a collapsed structure. For the CEL-Na-HPMCAS ASSD, spherical particles were observed with irregular surfaces, whereas the CEL-HPMCAS ASD showed irregular shaped particles which were collapsed and highly engraved. The ASSDs prepared with the K^+ counterion showed spherical particles with collapsed structures on the surface. The morphology of the CEL-K-HPMCAS ASSD was more irregular due to highly collapsed surface which may be due to evaporation of solvent from the surface as well as from the core of the particles during spray drying. In the ASSD formulations, the higher solute concentration in the droplets might have led to the faster drying of particles, and the vapor pressure due to the solvent produced smoother particles. On the other hand, a relatively slow rate of solvent evaporation, because of the lower solute content in the drying droplets, might have resulted in shrinkage of the particles, leading to the generation of rough surfaces in the ASDs.

DISCUSSION

The development of next generation ASDs for enhancing the solubility of PWSDs is much needed due to problems of dose dumping and low drug loading capacity, which lead to adverse side-effects, high dosage regimens, and increased overall costs of therapy. Here, we developed advanced ASDs, namely amorphous salt solid dispersions (ASSDs), of CEL, a widely used anti-inflammatory drug that is a PWSD. These ASSDs alleviate many of the problems of conventional ASDs. Although it is established that polymers and salts can play an important role in solubilizing and stabilizing PWSDs, the detailed mechanisms governing the properties of ASDs are poorly understood. The effect of polymers on intermolecular drug-drug interactions in both ionic and neutral states of the drug in aqueous phase are largely unexplored and the basis for the selection of an optimal salt-polymer combination for a particular drug is unclear. Therefore, we here performed *in silico* MD simulations of drug-salt-polymer systems in an aqueous environment and compared the results to experimental measurements of *in vitro* properties and the *in vivo*

565 fate of the drug. Atomic detail MD simulations of such systems have only recently
566 become feasible due to the large size and chemical heterogeneity of excipient polymers,
567 making it necessary to simulate systems with large numbers of atoms for long times to
568 obtain sufficient sampling. Thus, the MD simulations were carried out to explore the
569 effects of polymers and ions on drug-drug interactions and drug aggregation, but drug
570 crystallization processes were not simulated as they take place on much longer timescales
571 than the nano-microsecond durations of the MD simulations.
572 We focused on ASDs containing CEL, and one of two established polymer excipients -
573 PVP-VA or HPMCAS - with or without Na^+ or K^+ salts. While classical empirical models
574 showed adequate miscibility of CEL and both polymers, they were unable to identify the
575 best drug-salt-polymer combination. In contrast, more stable drug-polymer intermolecular
576 interaction energies computed from the atomically detailed MD simulations were found to
577 correlate with prolonged stability of supersaturated amorphous drug-salt-polymer systems.
578 MD simulations revealed that the PVP-VA oligomer formed a relatively more stable
579 complex with anionic CEL than the neutral form and was found to be a better candidate
580 than HPMCAS in inhibiting precipitation and maintaining supersaturation of CEL for a
581 prolonged time. All simulations of CEL-containing systems were performed in the
582 presence of NaCl and, as no effects of the Na+ ions on the CEL:CEL or CEL:oligomer
583 interactions were observed, similar behaviour would be expected in simulations with K+
584 ions. However, some differences in solubility were observed experimentally between
585 ASSDs with the two cations, likely due to the lower polarizability of K+ compared to Na+
586 ions. Thermal stability analysis and various *in vitro* and *in vivo* studies were performed,
587 which revealed that the CEL-Na-PVP-VA and CEL-K-PVP-VA formulations exhibited
588 higher glass transition temperature (T_g) values, proffering good physical stability, along
589 with improved biopharmaceutical performance. This novel technology of amorphous
590 formulation of CEL facilitates *in situ* salt formation within the polymer matrix leading to
591 high drug-loading and prolonged stability, along with ameliorated aqueous solubility,
592 dissolution, and pharmacokinetic profiles, offering the prospect of less frequent
593 administration and lower doses with good patient compliance, and therefore fewer side
594 effects.
595 It should be noted that the ASSD technology is not suitable for non-ionizable drugs due to
596 their inability to form a salt. In addition, due to the higher hygroscopicity of ASSDs
597 because of salt formation in comparison to ASDs, their applicability could be challenging
598 for more hygroscopic drugs. The ASSD technology remains to be explored for
599 permeability enhancement of biopharmaceutical classification system (BCS) class IV
600 drugs, that have both low permeability and low solubility. Despite such limitations, the
601 ASSD technology has potential for the formulation of ~ 40 % of marketed drugs and ~90
602 % of molecules in the drug discovery pipeline that are poorly water soluble and have
603 compromised bioavailability.
604 The PVP-VA ASSDs characterized in this work may, upon further development for
605 industrial production, find direct application for the administration of CEL due to their
606 excellent biopharmaceutical properties and cost-effectiveness compared to formulations
607 currently in use. Indeed, a straightforward scale-up for their production should be feasible.
608 Although we only considered one drug and a limited number of polymer-salt
609 combinations in this study, the combined computational and experimental approach
610 described here is generally applicable to other class of drugs and polymer types and can be
611 used to aid the rational choice of drug-salt-polymer combinations for drug formulation.
612 Moreover, we expect the physical insights gained into the determinants of amorphous
613 formulations to be relevant for the design of drug-salt-polymer combinations for the
614 formulation of the large class of PWSDs. Finally, the ASSD technology could pave the

way for biowaivers due to the immediate release of more than 85 % of the drug from the ASSD formulations within 15 to 30 minutes of dissolution, as required by USFDA guidelines for immediate-release drug products[54]; this would provide the dual benefit of cost and time by circumventing the need for *in vivo* bioequivalence studies.

MATERIALS AND METHODS

Experimental design. The experimental and computational characterizations of the systems studied were performed in parallel and the results compared. The systems were chosen to allow systematic comparison of the effects of two polymers – HPMCAS and PVP-VA in the presence or absence of Na^+ or K^+ salts on the physicochemical and biopharmaceutical properties of CEL when formulated as amorphous (salt) solid dispersions. The experiments were designed with the aim of identifying the determinants of system behaviour at supersaturation in aqueous phase and of drug bioavailability.

Materials. CEL form III was provided as a gift sample by Jubilant Generics Ltd. (Noida, Uttar Pradesh, India). PVP-VA, manufactured by BASF (Germany) and HPMCAS-MF grade, manufactured by Shin Estu (Japan) was generously provided by Signet Chemical Corporation Pvt. Ltd. (Mumbai, India). NaOH and KOH were procured from Himedia Laboratories Pvt. Ltd. (Mumbai, India). All other chemicals used in the experiments were of analytical grade and used as such.

Determination of drug-polymer miscibility. Estimation of δ by the Fedors and HVK methods is the conventional approach to calculate drug-polymer miscibility in order to prepare thermodynamically stable amorphous solid based formulations[55, 56]. The drug and polymer are found to be miscible if both have similar δ values with the difference in the solubility parameters (Δδ) being less than 7 $MPa^{1/2}$. The Hildebrand solubility parameter for the CEL-PVP-VA and CEL-HPMCAS systems was calculated using Fedors method from the cohesive energy density (CED) using Equation 1, where E_v is the energy of vaporization, V_m is the molar volume, and CED is the cohesive energy per unit volume[55]. The HVK method considers the dispersive forces, interactions between polar groups, and hydrogen bonding groups as shown in Equation 2, where δ_d, δ_p and, δ_h are the dispersive, polar, and hydrogen bonding solubility parameter components, respectively. These components can be further calculated using Equation 3, where F_{di} (dispersion component), F_{pi} (polar component) and E_{hi} (hydrogen bonding energy) are the group contributions for different components of structural groups and V is the group contribution to molar volume[55]. Further, the lattice-based F-H interaction parameter, χ was estimated using the δ value describing the change in Gibbs free energy before and after mixing of drug and polymer as shown in Equation 4, where χ refers to the square of the difference in δ value of the drug and the polymer, calculated from group contribution methods at 25 °C, R is the gas constant, T is the absolute temperature, and V_{site} is the volume per lattice site[55].

$$\boldsymbol{\delta = (CED)^{0.5} = \left(\frac{\Delta E_v}{V_m}\right)^{0.5}} \quad \textbf{(1)}$$

$$\boldsymbol{\delta_{Coh}^2 = \delta_d^2 + \delta_p^2 + \delta_h^2} \quad \textbf{(2)}$$

$$\boldsymbol{\delta_d = \frac{\sum F_{di}}{V},\ \delta_p = \frac{\sqrt{\sum F_{pi}^2}}{V},\ \delta_h = \sqrt{\frac{\sum E_{hi}}{V}}} \quad \textbf{(3)}$$

$$\chi = \frac{V_{site}(\delta_{drug} - \delta_{polymer})^2}{RT} \quad \text{.....(4)}$$

Generation of ASSD and binary ASD formulations. The generation of ASSD formulations was previously explained in detail[27]. Briefly, CEL (pKa 11.1) and counterions {K^+ (KOH (pKa 14.7)) or Na^+ (NaOH (pKa 15.7))} were dissolved in methanol in a 1:1 molar ratio to generate Na^+ and K^+ salt solutions. The salt formation is attributable to the pKa difference of more than 2 between CEL and the counterions. The two screened polymers, HPMCAS and PVP-VA, were dissolved separately in another part of methanol. The salt-containing solutions were then separately added to each polymer-containing solution in order to obtain a drug-polymer mass ratio of 6:4, and mixed well by magnetic stirring (see Fig. S1). The resulting solutions were then subjected to drying using a laboratory scale spray dryer (Buchi B-290, mini spray dryer, Buchi Labortechnik AG, (Switzerland)) set at the parameters of inlet temperature 80 °C, outlet temperature 50 °C, feed pump 12%, aspiration 85%, and air atomization pressure 400 L/h. Binary ASDs were also generated using the same technique by mixing CEL and HPMCAS or PVP-VA in a 6:4 ratio in methanol, and then spray drying.

Characterization methods. The concentration of CEL in samples for solubility and dissolution studies was analysed using a validated high-performance liquid chromatography (HPLC) method employing an HPLC system (Shimadzu Corporation, Kyoto, Japan) with a PDA detector (SPD- M10AVP) and LC solution software as described previously [27]. Optical imaging of powder samples was carried out to determine the morphology using a polarized light microscope (Leica Microsystems GmbH, (Wetzlar Germany)), and photomicrographs were acquired in both optical and polarised modes at 20x magnification using Leica IM 50 (version 1.20) software to determine the crystalline or amorphous nature of samples. The nature of the samples was also confirmed by DSC and PXRD. The sample preparation for DSC studies was done as described previously[27]. A Q2000 DSC (TA Instruments, New Castle, Delaware, USA) with an attached refrigerated cooling system and operating with Universal Analysis software version 4.5A (TA Instruments, (New Castle, Delaware, USA)) was used. Dry nitrogen at a 50 mL/min flow rate was used to purge the sample cell. The instrument was calibrated for temperature and heat flow using a high purity indium standard. Accurately weighed samples (4-5 mg) in aluminium pans were analysed by heating at a rate of 20 °C/min from 25 °C to 200 °C. The T_g and endothermic transitions were reported as the midpoint temperatures. Powder X-ray diffractograms for crystalline CEL and the generated ASSDs and ASDs were acquired at ambient conditions employing a Rigaku Ultima IV fully automatic high resolution X-ray diffractometer system (Rigaku Corporation, (Tokyo, Japan)) equipped with an X-ray radiation source Cu Kα tube at 1.54 Å wavelength that was operated at 40 kV/40mA, with a divergent slit of 0.5°, a divergent height limit slit of 10 mm, a scattering slit (SS) of 8.0 mm, and a receiving slit (RS) of 13 mm. All the samples were scanned continuously at a step size of 0.02° and scan rate of 15 seconds, over the range from 3° to 50° at an angle 2θ.

The molecular level drug-polymer interactions in the prepared formulations were investigated using the following high-end analytical techniques. FTIR spectra were recorded on an FTIR multiscope spectrophotometer (PerkinElmer, (Buckinghamshire, UK)) equipped with spectrum v3.02 software by a conventional KBr pellet method. The Micro-Raman Jobin Yvon HORIBA LABRAM HR-800 visible system (Kyoto, Japan) equipped with a 473 nm diode laser source, 1800 lines/mm grating, and an Olympus BX41 microscope was used to perform Micro-Raman spectroscopy. Raman spectra were recorded in back-scattering mode at room temperature with a pinhole size of 50 µm, slit width of 100 µm and exposure time of 10 seconds. Proton NMR was carried out for all the

samples dissolved in deuterated DMSO-d6 using a Bruker 500 UltraShield NMR spectrometer (Billerica, Massachusetts, USA) functioning at 500 MHz. Supersaturation and precipitation studies were conducted with a UV spectrophotometer (SpectraMax® M2 series) and software SoftMax Pro 6.2.1 (Molecular Devices, United States). The sample was immersed in 25 mL of water (aqueous media) at 37 °C for 4 hours by cuvette method. Plain crystalline CEL previously dissolved in methanol at 5 mg/mL concentration and drug-polymer samples (ASSD and binary ASD) containing the equivalent of 5 mg CEL were added to the aqueous media while stirring with a magnetic stirrer and the samples were analysed at the absorbing wavelength of 252 nm at reading intervals of 30 seconds.

Molecular modelling. The drug-polymer interplay at the molecular level was further elucidated by MD simulation to address the role and specificity of the polymer in preventing drug-drug aggregation in supersaturated systems. MD simulations were performed for both neutral and anionic CEL in the presence and absence of polymers, estimating the interaction energies between oligomer:CEL and CEL:CEL complexes. The molecular models of CEL, PVP-VA and HPMCAS were generated for further simulation studies. The coordinates of the neutral form of CEL were retrieved from the crystal structure in the Cambridge Crystallographic Data Centre (CCDC)[46, 57]. To model the anionic state of CEL, a hydrogen atom was removed from the sulfonamide group. A PVP-VA 34-mer (Fig. 1B) was generated using Materials Science (Schrödinger version 2020) by randomly assembling 18 units of vinylpyrrolidone (VP) and 16 units vinyl acetate (VA). The mass-ratio of these two units (VP:VA) in the model polymer was roughly equivalent to 6:4. A model of a hypromellose (HPMC) 20-mer was kindly provided by Prof. Ronald G. Larson, (Department of Chemical Engineering, University of Michigan, Ann Arbor, Michigan 48109-2136, USA). We removed 5 monomeric units and then converted the side chain hydroxyl (-OH) group of HPMC to acetyl, deprotonated succinoyl, methoxy and hydroxypropoxy groups using Maestro (Schrödinger version 2020) to build a HPMCAS 15-mer. We chose the side-chain substitutions corresponding to the composition of M-grade HPMCAS[58] (Fig. 1C). Consequently, the modelled 15-mer-M-grade HPMCAS polymer contained 45 substituents having 5 different functional groups in the following proportions (given as % of the number of functional groups and by weight (%wt)): methoxy (64.4%; 25%wt), hydroxypropoxy (8.9%; 8.3%wt), acetyl (11.1%; 8.3%wt), succinate (8.9%; 13%wt) and hydroxyl groups or no substitution (6.7%; 1.3%wt).

Molecular parameterization. GAFF[59] parameters were assigned to CEL and the polymers. Partial atomic charges for both CEL and the polymers were generated by the RESP[60] method as implemented in Antechamber in the AMBER version 14 software package[61] with the Gaussian 09[62] software with B3LYP-6-31G*/HF-6-31G* level of theory[63-66] being used for the electrostatic potential (ESP) calculations. For the polymers, geometry optimization followed by ESP calculations for the entire oligomers would be too computationally demanding. Therefore, RESP charges were computed for each monomeric unit separately. For this purpose, the monomeric units were built with blocking groups to account for the adjacent units. For PVP-VA, six non-terminal and two terminal (see Fig. S9) monomeric units were modelled. Likewise, for HPMCAS (Fig. 1C), 13 non-terminal monomeric units were generated by adding an isopropyl group to each of the two terminal oxygen atoms, and 2 terminal monomeric units were generated by adding an isopropyl group to the first and last terminal oxygen atom of HPMCAS. To maintain charge neutrality of the oligomers, the residual charge (-1.646e for the PVP-VA 34-mer and +1.926e for the HPMCAS 15-mer) after assigning the RESP charges to the monomers, which is due to the capping of the terminal atoms of the monomers, was

distributed equally onto all the atoms in the oligomers. The TIP3P[67] model was used for water molecules.

Refinement of polymer models by MD simulation. To structurally refine the polymer models, all-atom MD simulations in explicit solvent were carried out for the two representative model structures of PVP-VA and HPMCAS. The polymers were immersed in cubic periodic boxes using the Gromacs[68] insert-molecules command and then TIP3P water molecules were added to the system using the tleap module of AMBER. To avoid periodicity artifacts, the box dimensions were greater than the lengths of oligomers (see Table 1). 4 excess Na+ ions were added to neutralize the HPMCAS oligomer. The MD simulation protocol is given below. The last snapshot from each trajectory was extracted and used as the starting structure for drug-polymer simulations. The simulation lengths, box sizes and the numbers of water, ions are listed in Table 2 (systems a and b).

Simulation of CEL aggregation. To simulate a supersaturated solution of CEL, we generated periodic boxes with the same number of CEL molecules as used for the drug-oligomer systems described below. 11 and 13 CEL molecules, which were modelled in either neutral or anionic forms, were inserted randomly in cubic periodic boxes of water molecules with a box-length of 106 and 112 Å, respectively, using the Gromacs insert-molecules and gmx solvate commands. Na^+ ions were added to neutralize each system and thus the Na^+:CEL mass-ratio for each simulated system with anionic CEL molecules was 0.0603:1, while in the experiments, the NaOH:CEL ratio was 0.105:1. Note that the hydroxide anions (OH^-) are expected to extract the proton from the CEL sulfonamide nitrogen at higher pH values, and therefore the simulated systems did not contain hydroxide ions. In addition, further Na^+ and Cl^- ions were added to all the simulation boxes to generate ~0.01M ionic solutions (see Table 2). Then, the hydrogen atoms of the water molecules were removed and the residue name of water changed to WAT and the entire system was input to tleap to set it up for simulation with AMBER. All-atom explicit solvent energy minimization and MD simulations were carried out for all the systems and the aggregation of CEL was monitored. The simulation lengths, box sizes and the numbers of water, ions are given in Table 2 (systems c-f).

Simulation of CEL-polymer systems. For each of the CEL-oligomer combinations listed in Table 2 (systems g-j), one oligomer and several CEL molecules were placed randomly in a periodic simulation box using the Gromacs insert-molecules command, followed by packing of the boxes with water molecules and ions using the gmx solvate command. A typical dose of CEL is 100 to 200 mg given BD (twice a day) with or without food (https://go.drugbank.com/drugs/DB00482). The water content in an empty stomach is typically 35 ml[69].Thus, the stomach is a supersaturated system with CEL concentration of 1731.6 times higher than its experimental equilibrium solubility (3.46 mg/L)[27]. The molecular weights of the model PVP-VA 34-mer, M-grade HPMCAS 15-mer, and CEL are 3375.5, 3691.5, and 381.3 Da, respectively. Hence, to mimic the situation in the experiments, the CEL:oligomer mass ratio in our model systems was chosen to be 1:0.68 for PVP-VA and 1:0.88 for HPMCAS. Thus, one PVP-VA 34-mer and 13 CEL molecules were inserted in a cubic box of length 112 Å, and one HPMCAS 15-mer and 11 CEL molecules were inserted in a cubic box of length 106 Å. Afterwards, Na^+ and Cl^- ions were added (see Table 2), and the systems were re-solvated with the tleap module of AMBER as aforementioned and then, all atom explicit solvent energy minimization followed by MD simulations and post-facto trajectory analysis were performed.

MD simulation protocols. All the systems were energy minimized using the AMBER v14 and v20 software[60]. Energy minimization was carried out by restraining non-hydrogen solute atoms with a force constant that gradually decreased from 1000 to 0 kcal/mol·Å^2. During energy minimization, the maximum number of cycles was set to 14000 steps: 1400 steps steepest descent followed by 12600 steps conjugate gradient. Minimization was stopped when the root mean square energy gradient for the input coordinates was less than 0.00001 kcal/mol/Å.

MD equilibration and production runs were performed using the AMBER v20 software starting with the energy minimized coordinates. Each system was first equilibrated at constant volume and temperature (NVT) (with the AMBER parameter NTB=1) for a total of 16 ns with a time step of 2 fs at 300 K using the Particle Mesh Ewald (PME) method for long range electrostatic interactions with a non-bonded cut-off of 10 Å. The SHAKE algorithm[70] was imposed to constrain all the bonds to hydrogen atoms. The Langevin dynamics method with a damping coefficient of 5/ps was used for temperature control. The first 6 ns of equilibration was carried out by gradually reducing the restraint force constant from 100 to 10 kcal/mol·Å^2 on all non-hydrogen solute atoms. Then the remaining 10 ns of equilibration were run without harmonic restraints. The subsequent production runs were performed for times depending on the convergence of structural parameters, with a time step of 2 fs and a temperature of 300 K in an NPT ensemble (constant number of particles, pressure and temperature were maintained). All simulations were run in duplicate with the same initial coordinates but with different velocities assigned. Coordinates were written at 2.5 ps intervals throughout the simulations.

Analysis of MD trajectories. Analysis of the trajectories was performed using AMBER CPPTRAJ[71]. The RMSD was computed for the frames collected along the simulations and hydrogen bond and radial distribution function (RDF) analysis was carried out for the fully equilibrated part of the trajectories. MM/GBSA solvation and interaction free energy[72, 73]calculations were carried out for frames extracted at 100 ps intervals from the same equilibrated parts of the trajectories (Table 1). To compute the drug-drug aggregation energy using the MM/GBSA method, for each extracted frame, we considered each CEL molecule, one at a time, in the drug aggregate (ith celecoxib where "i" is an integer number) and then computed the interaction energy between this molecule and the rest of the aggregate. The CEL-CEL interaction energy was the value computed by averaging over all the CEL molecules in the simulated system and over all the extracted frames. The CEL-oligomer interaction energy was estimated similarly by, for each frame, computing the interaction energy of each CEL molecule with the rest of the complex, i.e.; oligomer and all the remaining CEL molecules, and then subtracting the CEL:CEL aggregation energy from the energy of the CEL:oligomer-CEL system to give the CEL:oligomer interaction energy. The final CEL-oligomer interaction energy was then obtained as the average interaction energy over all frames and overall CEL molecules for each replica trajectory. The average and standard deviation of the MM/GBSA interaction free energy over the replicas was then computed.

Xmgrace (plasma-gate.weizmann.ac.il/Grace/) was used for plotting. Molecular visualization was performed with PyMOL (https://pymol.org/2/) or VMD[74].

Apparent solubility and *in vitro* dissolution studies. Apparent solubility studies were carried out in distilled water, maintained at 37 ± 0.5 °C using a shaking water bath operated at 100 rpm. An excess amount of solid (20 mg) was added to 15 mL of water and aliquots of 1 mL were withdrawn at predetermined time points up to 6 h. All the samples were immediately centrifuged at 15,000 rpm for 10 min and the supernatant was collected for analysis. *In vitro* dissolution studies were conducted for the prepared ASSD

formulations, the binary ASDs, the physical mixture (PM) [of CEL, polymers and NaOH/KOH mixed geometrically in a mortar using a spatula], and crystalline CEL using a tablet dissolution apparatus (USP 37, type II) (TDT-08L, Electrolab, (Mumbai, India)) with an autosampler. The dissolution medium used was 0.04 M tribasic sodium phosphate at pH 12 (under sink conditions) [recommended by the Office of Generic Drugs (OGD), USFDA] and at pH 11 (under non-sink conditions) without surfactant (SLS). A dose equivalent to 100 mg of CEL was added to 1000 ml of dissolution medium maintained at 37 ± 0.5 °C and at 50 rpm. A sample volume of 5 mL was withdrawn at predetermined time intervals up to 120 min, filtered through a 0.22 µm syringe filter (Nylon, MDi membrane filters, Advanced Microdevices Pvt. Ltd., (Ambala Cantt, India)), and the same volume of dissolution medium was supplied instantly after sample withdrawal to maintain sink conditions, whereas no replacement of media was done for non-sink conditions. The CEL concentration in the collected samples after suitable dilution for both solubility and dissolution studies was determined by the validated HPLC method detailed in Tables S3 and S4 and Fig. S13.

***In vivo* pharmacokinetic studies.** *In vivo* pharmacokinetic studies were conducted in SD rats (female, weight: 200 ± 30 g). The CPCSEA (Committee for the Purpose of Control and Supervision of Experiments on Animals) guidelines were followed for performing animal studies. The protocol for animal studies (IAEC/19/51-R) was sanctioned by the Institutional Animal Ethics Committee, NIPER, Mohali, India. All the animals were exposed to 12 h light-dark cycles at 25 °C and 60 % RH for one week and were fasted for 12 h with free access to water before the start of experiments. 7 groups, each consisting of 5 animals, were used for testing seven formulations viz. CEL-Na-PVP-VA and CEL-K-PVP-VA; ASSD, CEL-Na-HPMCAS and CEL-K-HPMCAS; ASSD, binary CEL-PVP-VA and CEL-HPMCAS; ASD, and pure crystalline CEL. All formulations were administered orally via oral gavage at a dose of 10 mg equivalent of CEL/kg of rat body mass. Blood samples of approximately 150-200 µL were collected from the tail vein at predetermined time points up to 48 h. Plasma was separated from the blood samples by centrifugation at 10,000 rpm for 10 min at 4 °C and stored at −40 °C before analysis. The pharmacokinetic parameters, C_{max}, T_{max}, mean residence time (MRT) and $t_{1/2}$, were derived from the mean plasma concentration−time profiles using the Thermo Kinetica software (V5.0, Thermo Fischer Scientific, USA).

Stability studies. ASSDs and binary ASDs were evaluated for physical stability at ambient conditions in closed containers. Samples were evaluated by polarised light microscopy for detection of birefringence, and by DSC for detecting melting endotherm, indicating the presence of crystallinity in amorphous formulations.

Scanning electron microscopy (SEM). SEM studies were performed for generated ASSDs and ASDs. The surface morphology of powder samples was viewed under a scanning electron microscope (S-3400, Hitachi Ltd., Tokyo, Japan) operated at an excitation voltage of 25 kV. The powder samples were mounted onto a steel stage using double-sided adhesive tape and sputter-coated with gold using ion sputter (E-1010, Hitachi Ltd., Tokyo, Japan), before analysis.

Statistical analysis. The statistical data analysis was done by one-way analysis of variance (ANOVA) using GraphPad Prism 9 software, version 9.1.0 (221) (GraphPad Software, LLC. San Diego, USA). The results were considered statistically significant when $p < 0.05$.

REFERENCES

1. J. P. Lakshman, Y. Cao, J. Kowalski, A. T. M. Serajuddin, Application of melt extrusion in the development of a physically and chemically stable high-energy amorphous solid dispersion of a poorly water-soluble drug. *Mol. Pharm.* **5**, 994-1002 (2008).

2. L. S. Taylor, G. G. Z. Zhang, Physical chemistry of supersaturated solutions and implications for oral absorption. *Adv. Drug Del. Rev*. **101,** 122-142 (2016).

3. S. V. Bhujbal, B. Mitra, U. Jain, Y. Gong, A. Agrawal, S. Karki, L. S. Taylor, S. Kumar, Q. T. Zhou, Pharmaceutical amorphous solid dispersion: a review of manufacturing strategies. *Acta Pharm. Sin. B.* **11**, 2505-2536 (2021).

4. L. A. Wegiel, L. J. Mauer, K. J. Edgar, L. S. Taylor, Crystallization of amorphous solid dispersions of resveratrol during preparation and storage-impact of different polymers. *J. Pharm. Sci.* **102,** 171-184 (2013).

5. Y. Javadzadeh, S. M. Dizaj, Z. Vazifehasl, M. Mokhtarpour, Recrystallization of drugs-effect on dissolution rate. *Recryst. Mater. Processing* **191**, 211 (2015).

6. P. Joshi, P. Mallepogu, H. Kaur, R. Singh, I. Sodhi, S. K. Samal, K. C. Jena, A. T. Sangamwar, Explicating the molecular level drug-polymer interactions at the interface of supersaturated solution of the model drug: Albendazole. *Eur. J. Pharm. Sci.* **167**, 106014 (2021).

7. D. B. Warren, H. Benameur, C. J. H. Porter, C. W. Pouton, Using polymeric precipitation inhibitors to improve the absorption of poorly water-soluble drugs: a mechanistic basis for utility. *J. Drug Target.* **18,** 704-731 (2010).

8. S. Metre, S. Mukesh, S. K. Samal, M. Chand, A. T. Sangamwar, Enhanced biopharmaceutical performance of rivaroxaban through polymeric amorphous solid dispersion. *Mol. Pharm.* **15**, 652-668 (2018).

9. V. R. Wilson, X. Lou, D. J. Osterling, D. F. Stolarik, G. J. Jenkins, B. L. B. Nichols, Y. Dong, K. J. Edgar, G. G. Z. Zhang, L. S. Taylor, Amorphous solid dispersions of enzalutamide and novel polysaccharide derivatives: investigation of relationships between polymer structure and performance. *Sci. Rep.* **10**, 18535 (2020).

10. E. J. A. Suys, D. K. Chalmers, C. W. Pouton, C. J. H. Porter, Polymeric precipitation inhibitors promote fenofibrate supersaturation and enhance drug absorption from a type iv lipid-based formulation. *Mol. Pharm.* **15**, 2355-2371 (2018).

11. A.-R. Ilie, B. T. Griffin, M. Vertzoni, M. Kuentz, R. Kolakovic, A. Prudic-Paus, A. Malash, H. Bohets, J. Herman, R. Holm, Exploring precipitation inhibitors to improve in vivo absorption of cinnarizine from supersaturated lipid-based drug delivery systems. *Eur. J. Pharm.* Sci. **159,** 105691 (2021).

12. N. J. Koehl, L. J. Henze, H. Bennett-Lenane, W. Faisal, D. J. Price, R. Holm, M. Kuentz, B. T. Griffin, In silico, in vitro, and in vivo evaluation of precipitation inhibitors in supersaturated lipid-based formulations of venetoclax. *Mol. Pharm.* **18**, 2174-2188 (2021).

13. Z.-Q. Chen, Y. Liu, J. -H. Zhao, L. Wang, N.-P. Feng, Improved oral bioavailability of poorly water-soluble indirubin by a supersaturatable self-microemulsifying drug delivery system. *Int. J. Nanomed.* **7**, 1115-1125 (2012).

14. D. Feng, T. Peng, Z. Huang, V. Singh, Y. Shi, T. Wen, M. Lu, G. Quan, X. Pan, C. Wu, Polymer-surfactant system based amorphous solid dispersion: precipitation inhibition and bioavailability enhancement of itraconazole. *Pharmaceutics* **10**, 53 (2018).

15. A. Schittny, S. Philipp-Bauer, P. Detampel, J. Huwyler, M. Puchkov, Mechanistic insights into effect of surfactants on oral bioavailability of amorphous solid dispersions. *J. Control. Release* **320**, 214-225 (2020).

16. D. Clemett, K. L. Goa, Celecoxib: a review of its use in osteoarthritis, rheumatoid arthritis and acute pain. *Drugs* **59**, 957-80 (2000).

17. M. Dougados, J. M. Béhier, I. Jolchine, A. Calin, D. van der Heijde, I. Olivieri, H. Zeidler, H. Herman, Efficacy of celecoxib, a cyclooxygenase 2-specific inhibitor, in the treatment of ankylosing spondylitis: a six-week controlled study with comparison against placebo and against a conventional nonsteroidal antiinflammatory drug. *Arthritis Rheum*. **44**, 180-5 (2001).

18. M. M. Ward, Nonsteroidal anti-inflammatory drugs: disease modifiers in ankylosing spondylitis? *Nat. Clin. Pract. Rheumatol.* **1**, 18-19 (2005).

19. *Global Celecoxib Market Growth 2021-2026*. *Market Research Insights,* 130 https://www.marketreportsworld.com/enquiry/request-sample/19852767 (2021).

20. H. V. Nguyen, C. Park, E. Oh, B.-J. Lee, Improving the dissolution rate of a poorly water-soluble drug via adsorption onto pharmaceutical diluents. *J. Drug Deliv. Sci. Technol.* **35**, 146-154 (2016).

21. T. Cserháti, E. Forgács, G. Oros, Biological activity and environmental impact of anionic surfactants. *Environ. Int.* **28**, 337-48 (2002).

22. K. Kosswig, Surfactants. *Ullmann's Encycl. Ind. Chem*. **35**, 431-505 (2012).

23. H. J. Kwon, E. J. Heo, Y. H. Kim, S. Kim, Y. H. Hwang, J. M. Byun, S. H. Cheon, S. Y. Park, D. Y. Kim, K. H. Cho, H. J. Maeng, D. J. Jang, Development and evaluation of poorly water-soluble celecoxib as solid dispersions containing nonionic surfactants using fluidized-bed granulation. *Pharmaceutics* **11**, 136 (2019).

24. S. K. Paulson, M. B. Vaughn, S. M. Jessen, Y. Lawal, C. J. Gresk, B. Yan, T. J. Maziasz, C. S. Cook, A. Karim, Pharmacokinetics of celecoxib after oral administration in dogs and humans: effect of food and site of absorption. *J. Pharmacol. Exp. Ther.* **297,** 638-45 (2001).

25. J. W. J. Bijlsma, Celecoxib-fewer gastrointestinal adverse events in patients with osteoarthritis. *Nat. Clin. Pract. Rheumatol.* **2**, 414-415 (2006).

26. J. K. Aronson, COX-2 inhibitors (coxibs) *Meyler's Side Effects of Drugs*, 738-762 (2016).

27. S. Mukesh, P. Joshi, A. K. Bansal, M. C. Kashyap, S. K. Mandal, V. Sathe, A. T. Sangamwar, Amorphous salts solid dispersions of celecoxib: enhanced biopharmaceutical performance and physical stability. *Mol. Pharm.* **18**, 2334-2348 (2021).

28. R. Panakanti, A. S. Narang, Impact of excipient interactions on drug bioavailability from solid dosage forms. *Pharm. Res.* **29**, 2639-59 (2012).

29. Y. Ishizuka, K. Ueda, H. Okada, J. Takeda, M. Karashima, K. Yazawa, K. Higashi, K. Kawakami, Y. Ikeda, K. Moribe, Effect of drug-polymer interactions through hypromellose acetate succinate substituents on the physical stability on solid dispersions studied by fourier-transform infrared and solid-state nuclear magnetic resonance. *Mol. Pharm.* **16**, 2785-2794 (2019).

30. D. Yu, J. Li, H. Wang, H. Pan, T. Li, T. Bu, W. Zhou, X. Zhang, Role of polymers in the physical and chemical stability of amorphous solid dispersion: A case study of carbamazepine. *Eur. J. Pharm. Sci.* **169**, 106086 (2022).

31. D. D. Patel, B. D. Anderson, Effect of precipitation inhibitors on indomethacin supersaturation maintenance: mechanisms and modeling. *Mol. Pharm.* **11**, 1489-1499 (2014).

32. R. Singh, V. Thorat, H. Kaur, I. Sodhi, S. K. Samal, K. C. Jena, A. T. Sangamwar, Elucidating the molecular mechanism of drug-polymer interplay in a polymeric supersaturated system of rifaximin. *Mol. Pharm.* **18,** 1604-1621 (2021).

33. P. J. Marsac, T. Li, L. S. Taylor, Estimation of drug–polymer miscibility and solubility in amorphous solid dispersions using experimentally determined interaction parameters. *Pharm. Res.* **26**, 139 (2009).

34. F. Meng, V. Dave, H. Chauhan, Qualitative and quantitative methods to determine miscibility in amorphous drug–polymer systems. *Eur. J. Pharm. Sci.* **77,** 106-111 (2015).

35. C. Phadke, J. Sharma, K. Sharma, A. K. Bansal, Effect of variability of physical properties of povidone K30 on crystallization and drug-polymer miscibility of celecoxib-povidone K30 amorphous solid dispersions. *Mol. Pharm.* **16**, 4139-4148 (2019).

36. C. Li, J.-X. Wang, Y. Le, J.-F. Chen, Studies of bicalutamide-excipients interaction by combination of molecular docking and molecular dynamics simulation. *Mol. Pharm.* **10**, 2362-9 (2013).

37. J. Gupta, C. Nunes, S. Vyas, S. Jonnalagadda, Prediction of solubility parameters and miscibility of pharmaceutical compounds by molecular dynamics simulations. *J. Phys. Chem. B* **115**, 2014-2023 (2011).

38. W. Huang, I. S. Dalal, R. G. Larson, Analysis of solvation and gelation behavior of methylcellulose using atomistic molecular dynamics simulations. *J. Phys. Chem. B* **118**, 13992-14008 (2014).

39. Q. Li, Q. Zhao, Q. Jing, X. Ma, N. Chen, G. Ren, D. Ouyang, F. Ren, Investigating molecular interactions of high-loaded glipizide-HPMCAS microparticles by integrated experimental and modeling techniques. *Eur. J. Pharm. Sci.* **131**, 127-135 (2019).

40. W. Huang, T. Mandal, R. G. Larson, Computational modeling of hydroxypropyl-methylcellulose acetate succinate (HPMCAS) and phenytoin interactions: a systematic coarse-graining approach. *Mol. Pharm.* **14**, 733-745 (2017).

41. W. Huang, T. Mandal, R. G. Larson, Multiscale computational modeling of the nanostructure of solid dispersions of hydroxypropyl methylcellulose acetate succinate (HPMCAS) and phenytoin. *Mol. Pharm.* **14**, 3422-3435 (2017).

42. J. Dong, H. Gao, D. Ouyang, PharmSD: A novel AI-based computational platform for solid dispersion formulation design. *Int. J. Pharm.* **604**, 120705 (2021).

43. H. Gao, W. Wang, J. Dong, Z. Ye, D. Ouyang, An integrated computational methodology with data-driven machine learning, molecular modeling and PBPK modeling to accelerate solid dispersion formulation design. *Eur. J. Pharm. Biopharm.* **158**, 336-346 (2021).

44. D. B. Murphy, K. R. Spring, T. J. Fellers, M. W. Davidson, Principles of Birefringence [MicroscopyU]. https://www.microscopyu.com/techniques/polarized-light/principles-of-birefringence.

45. P. Gupta, R. Thilagavathi, A. K. Chakraborti, A. K. Bansal, Differential molecular interactions between the crystalline and the amorphous phases of celecoxib. *J. Pharm. Pharmacol.* **57**, 1271-8 (2005).

46. J. F. Remenar, M. D. Tawa, M. L. Peterson, Ö. Almarsson, M. B. Hickey, B. M. Foxman, Celecoxib sodium salt: engineering crystal forms for performance. *Cryst. Eng. Comm.* **13**, 1081-1089 (2011).

47. J. Mähler, I. Persson, A study of the hydration of the alkali metal ions in aqueous solution. *Inorg. Chem.* **51**, 425-438 (2012).

48. G. P. Andrews, O. Abu-Diak, F. Kusmanto, P. Hornsby, Z. Hui, D. S. Jones, Physicochemical characterization and drug-release properties of celecoxib hot-melt extruded glass solutions. *J. Pharm. Pharmacol.* **62**, 1580-90 (2010).

49. D. T. Friesen, R. Shanker, M. Crew, D. T. Smithey, W. J. Curatolo, J. A. S. Nightingale, Hydroxypropyl methylcellulose acetate succinate-based spray-dried dispersions: an overview. *Mol. Pharm.* **5**, 1003-1019 (2008).

50. A. T. M. Serajuddin, Salt formation to improve drug solubility. *Adv. Drug Deliv. Rev.* **59,** 603-616 (2007).

51. T. Školáková, M. Slámová, A. Školáková, A. Kadeřábková, J. Patera, P. Zámostný, Investigation of dissolution mechanism and release kinetics of poorly water-soluble tadalafil from amorphous solid dispersions prepared by various methods. *Pharmaceutics* **11**, 383 (2019).

52. A. Schittny, J. Huwyler, M. Puchkov, Mechanisms of increased bioavailability through amorphous solid dispersions: a review. *Drug Deliv*. **27**, 110-127 (2020).

53. L. Miao, Y. Liang, W. Pan, J. Gou, T. Yin, Y. Zhang, H. He, X. Tang, Effect of supersaturation on the oral bioavailability of paclitaxel/polymer amorphous solid dispersion. *Drug Deliv. Transl. Res.* **9**, 344-356 (2019).

54. N. H. S. Reddy, S. Patnala, R. Lobenberg, I. Kanfer, *In vitro* dissolution of generic immediate-release solid oral dosage forms containing BCS class I drugs: comparative assessment of metronidazole, zidovudine, and amoxicillin versus relevant comparator pharmaceutical products in South Africa and India. *AAPS PharmSciTech*. **15**, 1076-86 (2014).

55. D. W. Van Krevelen, K. T. Nijenhuis, Properties of polymers: their correlation with chemical structure; their numerical estimation and prediction from additive group contributions. 4th Edition, *Elsevier B.V.* (2009).

56. D. Medarević, J. Djuris, P. Barmpalexis, K. Kachrimanis, S. Ibric, Analytical and computational methods for the estimation of drug-polymer solubility and miscibility in solid dispersions development. *Pharmaceutics* **11**, 372 (2019).

57. C. R. Groom, I. J. Bruno, M. P. Lightfoot, S. C. Ward, The cambridge structural database. *Acta. Crystallogr. B. Struct. Sci. Cryst. Eng. Mater.* **72**, 171-179 (2016).

58. *AquaSolve*™ Hypromellose Acetate Succinate (HPMCAS) https://www.ashland.com/file_source/Ashland/Industries/Pharmaceutical/Links/PC-12624.6_AquaSolve_HPMCAS_Physical_Chemical_Properties.pdf, Ashland, Covington, KY, USA (2016).

59. J. Wang, R. M. Wolf, J. W. Caldwell, P. A. Kollman, D. A. Case, Development and testing of a general amber force field. *J. Comput. Chem.* **25**, 1157-74 (2004).

60. C. I. Bayly, P. Cieplak, W. Cornell, P. A. Kollman, A well-behaved electrostatic potential based method using charge restraints for deriving atomic charges: the RESP model. *J. Phys. Chem.* **97**, 10269-10280 (1993).

61. R. Salomon-Ferrer, D. A. Case, R. C. Walker, An overview of the amber biomolecular simulation package. *Wiley Interdiscip. Rev. Comput. Mol. Sci.* **3**, 198-210 (2013).

62. M. J. Frisch, G. W. Trucks, H. B. Schlegel, G. E. Scuseria, M. A. Robb, J. R. Cheeseman, G. V. Scalmani, B. Barone, G. A. Mennucci, H. Petersson, Gaussian 09, Revision E. 01, Gaussian. Inc., Wallingford CT, USA (2013).

63. W. J. Hehre, R. Ditchfield, J. A. Pople, Self—consistent molecular orbital methods. xii. further extensions of gaussian—type basis sets for use in molecular orbital studies of organic molecules. *J. Chem. Phys.* **56,** 2257-2261 (1972).

64. S. H. Vosko, L. Wilk, M. Nusair, Accurate spin-dependent electron liquid correlation energies for local spin density calculations: a critical analysis. *Can. J. Phys.* **58**, 1200-1211 (1980).

65. C. Lee, W. Yang, R. G. Parr, Development of the Colle-Salvetti correlation-energy formula into a functional of the electron density. *Phys. Rev. B Condens. Matter.* **37**, 785-789 (1988).

66. K. Raghavachari, Perspective on "density functional thermochemistry. III. the role of exact exchange", in theoretical chemistry accounts: new century issue. *Springer Berlin Heidelberg: Berlin, Heidelberg.* 361-363 (2001).

67. W. L. Jorgensen, J. Chandrasekhar, J. D. Madura, R. W. Impey, M. L. Klein, Comparison of simple potential functions for simulating liquid water. *J. Chem. Phys.* **79,** 926-935 (1983).

68. E. Lindahl, M. J. Abraham, B. Hess, D.V. Spoel, GROMACS development team, GROMACS 2021.2 Manual. https://manual.gromacs.org/2021.2/index.html, (2021).

69. D. M. Mudie, K. Murray, C. L. Hoad, S. E. Pritchard, M. C. Garnett, G. L. Amidon, P. A. Gowland, R. C. Spiller, G. E. Amidon, L. Marciani, Quantification of gastrointestinal liquid volumes and distribution following a 240 ml dose of water in the fasted state. *Mol. Pharm.* **11,** 3039-3047 (2014).

70. V. Kräutler, W. F. van Gunsteren, P. H. Hünenberger, A fast SHAKE algorithm to solve distance constraint equations for small molecules in molecular dynamics simulations. *J. Comput. Chem.* **22,** (2001).

71. D. R. Roe, T. E. Cheatham, PTRAJ and CPPTRAJ: software for processing and analysis of molecular dynamics trajectory data. *J. Chem. Theory Comput.* **9,** 3084-3095 (2013).

72. P. A. Kollman, I. Massova, C. Reyes, B. Kuhn, S. Huo, L. Chong, M. Lee, T. Lee, Y. Duan, W. Wang, O. Donini, P. Cieplak, J. Srinivasan, D. A. Case, T. E. Cheatham, Calculating structures and free energies of complex molecules: combining molecular mechanics and continuum models. *Acc. Chem. Res.* **33**, 889-897 (2000).

73. P. D. Lyne, M. L. Lamb, J. C. Saeh, Accurate prediction of the relative potencies of members of a series of kinase inhibitors using molecular docking and MM-GBSA scoring. *J. Med. Chem*. **49**, 4805-8 (2006).

74. W. Humphrey, A. Dalke, K. Schulten, VMD: visual molecular dynamics. *J. Mol. Graph.* **14**, 33-8, 27-8 (1996).

Acknowledgments

We thank Prajwal P. Nandekar for his contributions in the initial phases of this study, Giulia Paiardi for helpful discussions and assistance with data archiving, and Stefan Richter for technical support for the computational work.

Funding:
German Federal Ministry for Education and Research (BMBF) 01DQ19004 (RCW)
Klaus Tschira Foundation (GM, NS, CD, RCW)
Baden-Württemberg bwHPC for computing resources (RCW)
German Research Foundation (DFG) grant INST 35/1134-1 FUGG for computing resources (RCW)
Department of Biotechnology, New Delhi, BT/IN/BMBF-BioHR/34/ATS/2018-19 (ATS).

Author contributions:

Conceptualization: SM, GM, ATS, RCW

Experimental Investigation: SM, PJ

Computational Investigation: GM, NS, CD

Experimental Data Analysis: SM, RS, ATS

Computational Data Analysis: GM, NS, CD, RCW

Visualization: SM, RS, GM

Supervision: ATS, RCW

Writing—original draft, review and editing: SM, GM, RS, ATS, RCW

Competing interests: Authors declare that they have no competing interests.

Data and materials availability: All data are available in the main text or the supplementary materials or the repository at zenodo. Materials are available from the authors on reasonable request.

Figures and Tables

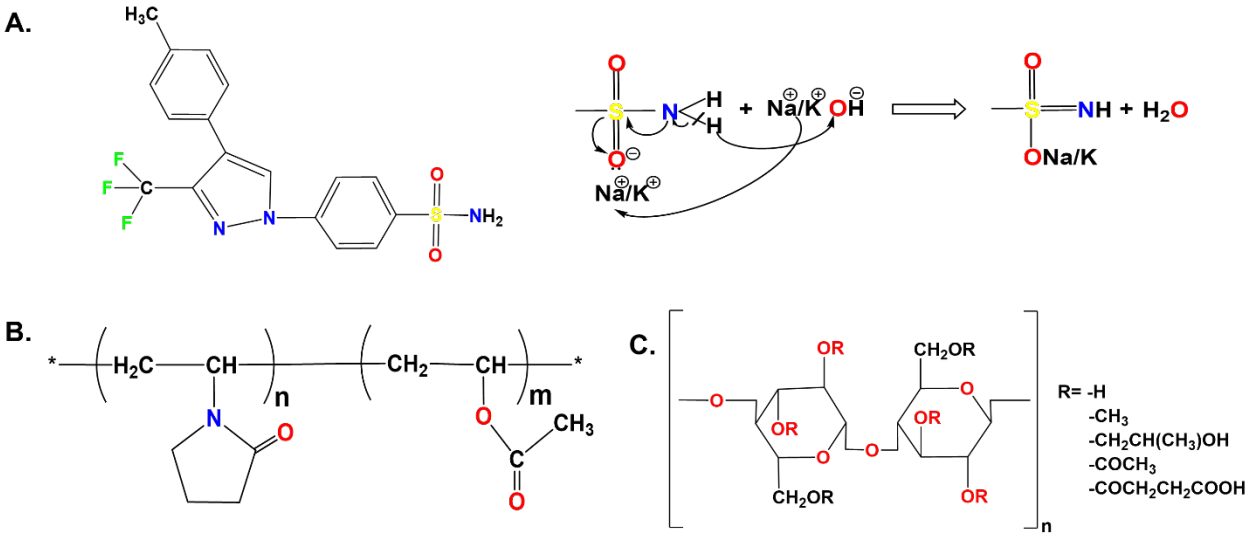

Fig. 1. Chemical structures of CEL and the polymer excipients studied. **(A)** CEL in neutral form with a scheme showing the formation of the CEL anionic salt in the presence of NaOH or KOH. **(B)** Poly-(1-vinylpyrrolidone-co-vinyl-acetate) (PVP-VA). (C) Hypromellose acetate succinate (HPMCAS). The M-grade contains acetyl and succinoyl groups at 7-11% and 10-14% weight fractions along with methoxyl and hydroxypropoxyl groups at 21-25% and 5-9%[58].

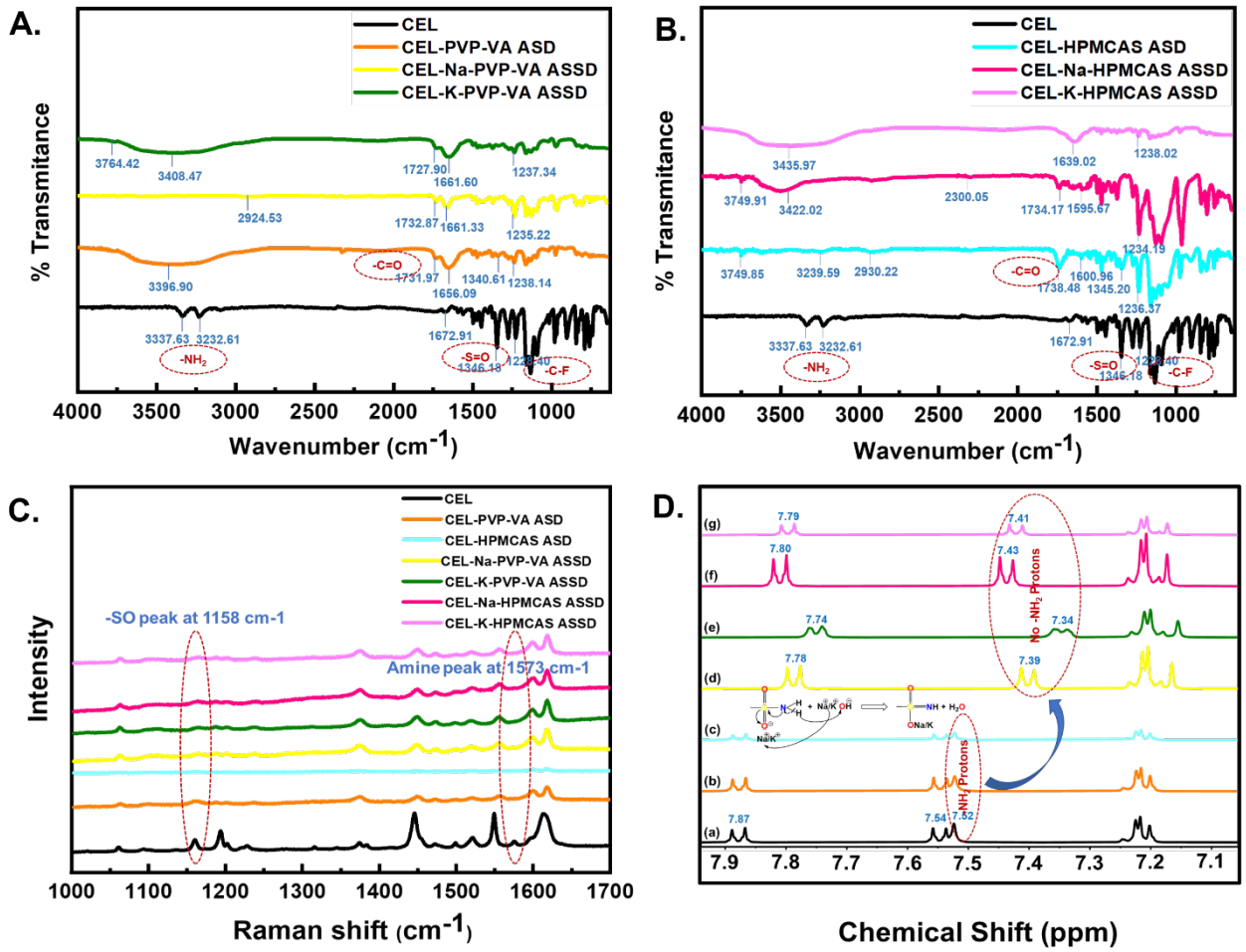

Fig. 2. Spectroscopic techniques reveal intermolecular interactions between CEL and the polymer in amorphous formulations. **(A,B)** FTIR-ATR spectra of CEL and CEL-PVP-VA (A) and CEL-HPMCAS (B) formulations. The spectra show the disappearance of the -S=O peak in ASSDs, indicating the involvement of the -S=O group in salt formation (Figure 1), and broadening of the -NH stretching peak of the $-NH_2$ group in ASDs and ASSDs, revealing the amorphous nature of both formulations. **(C)** Micro-Raman spectra of crystalline CEL and its ASD and ASSD formulations. The spectra for the ASSD formulations show the disappearance of the -S=O peak in the ASSD formations, indicating salt formation, and -NH stretching peak in both ASD and ASSD formulations, revealing the amorphous nature of the formulations. **(D)** NMR spectra between 7.1 and 7.9 ppm of (a) CEL, (b) CEL-PVP-VA ASD, (c) CEL-HPMCAS ASD, (d) CEL-Na-PVP-VA ASSD, (e) CEL-K-PVP-VA ASSD, (f) CEL-Na-HPMCAS ASSD and (g) CEL-K-HPMCAS ASSD. The complete spectral region is shown in Fig. S5. The spectra show the upfield shift in the aromatic protons of CEL at 7.87 and 7.54 ppm and the disappearance of the $-NH_2$ proton peak at 7.52 ppm in the ASSD formulations, indicating salt formation.

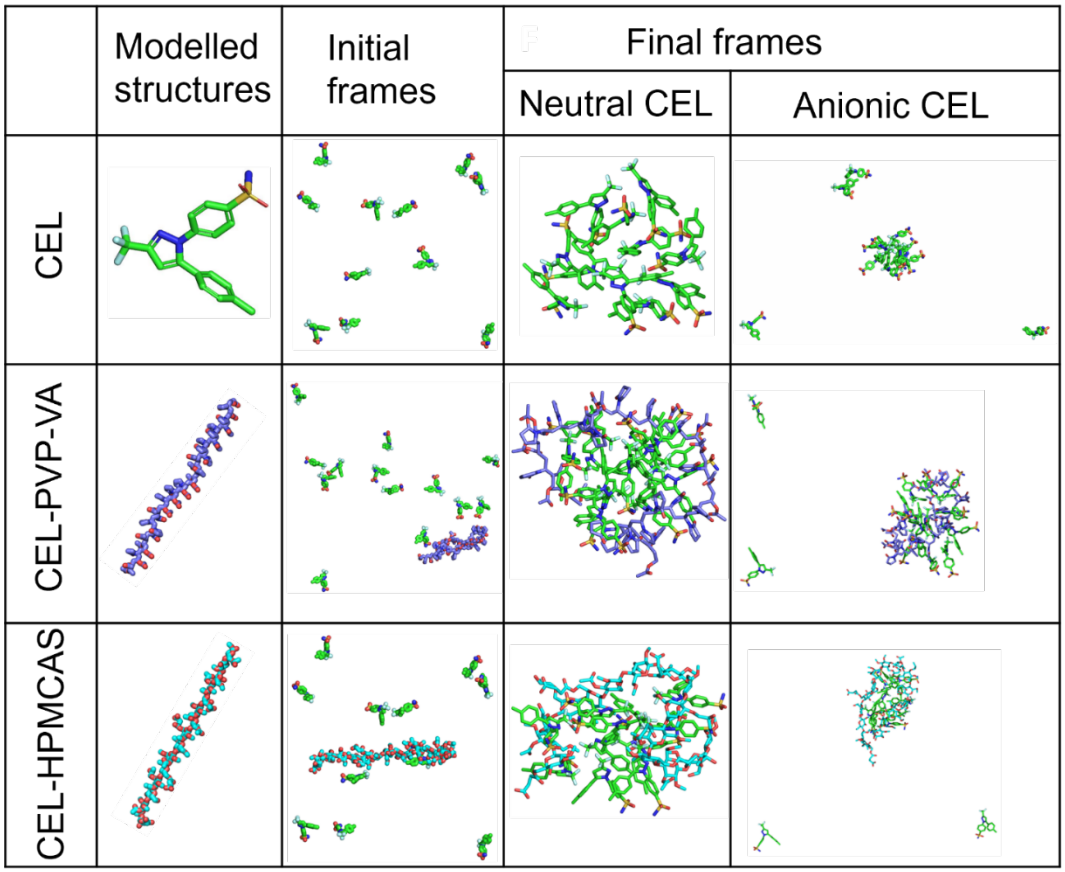

Fig. 3. Modelled structures of the molecules simulated and snapshots of initial and final frames of the simulated systems of CEL alone and CEL with either PVP-VA or HPMCAS. In the initial structures of the simulated systems, the CEL molecules were placed in random positions and orientations in a periodic box of solvent without or with an oligomer. The final frames of the systems simulated are for the simulation times given in Table 2 and shown for simulation replica-1 for systems with neutral or anionic forms of CEL. For the neutral form of CEL, aggregation of the CEL molecules alone or with the oligomer is observed during all the simulations. For the anionic form of CEL, a lower aggregation propensity was observed with some CEL molecules remaining free during the simulations (the final snapshot after simulation for 916 ns of system e for anionic CEL without oligomer is shown but in system f, which also lacked oligomer (Table 2), no aggregation of anionic CEL molecules was observed in a simulation of 1042 ns duration).

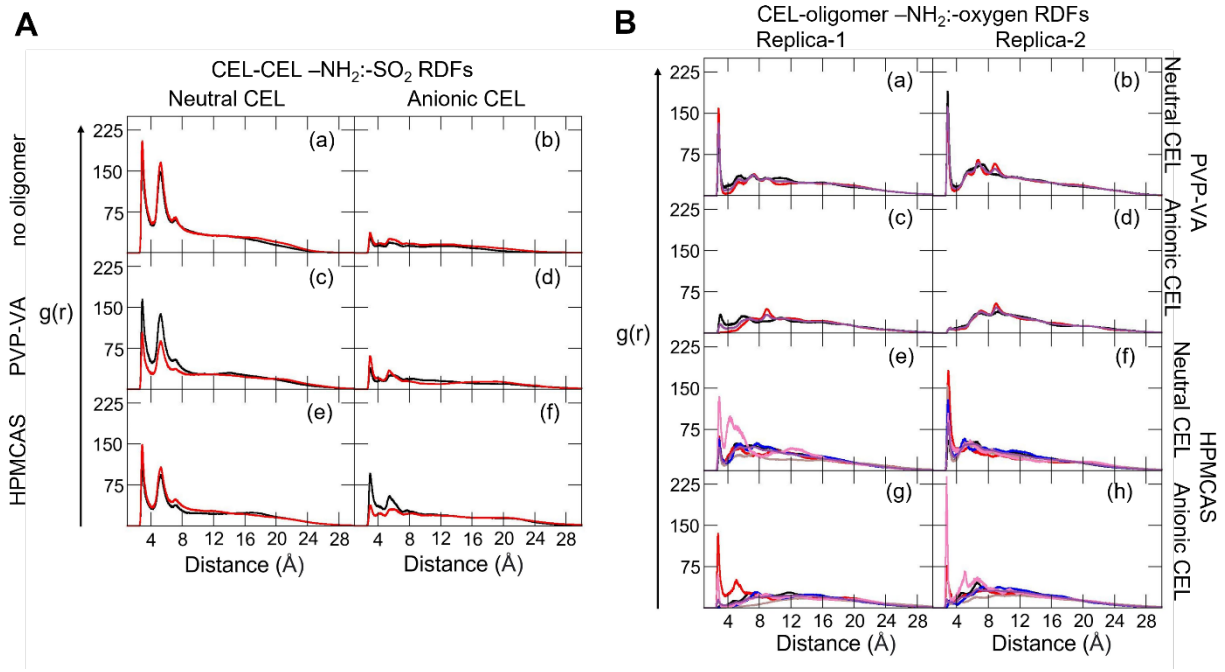

Fig. 4. Radial distribution functions (RDFs) computed from all-atom explicit solvent MD simulations showing CEL-CEL and CEL-oligomer intermolecular interactions. (A). Intermolecular CEL:CEL RDFs between the sulfonamide -NH_2 group of one CEL molecule and the SO_2 group of another (replica-1: black, replica-2: red) for the neutral (left) and anionic (right) forms of CEL without polymer (a,b), with PVP-VA (c,d), and with HPMCAS (e,f). The RDFs tend to zero with increasing distance because the molecules aggregate. **(B).** Intermolecular CEL:oligomer RDFs computed from the replica-1 (left) and replica-2 (right) MD simulations. RDFs are shown for: the sulfonamide -NH_2 group of the neutral (a,b) and anionic (c,d) forms of 13 CEL molecules and the carbonyl oxygen atoms of vinyl acetate (black) and vinylpyrrolidone (red) moieties and all oxygen atoms (purple) of the PVP-VA oligomer; sulfonamide -NH_2 group of neutral (e,f) and anionic (g,h) forms of 11 CEL molecules and oxygen atoms of methoxy (black), hydroxypropoxy (red), succinoyl (brown), acetyl (blue), hydroxy (pink) and all oxygen atoms (purple) of the HPMCAS oligomer.

1309

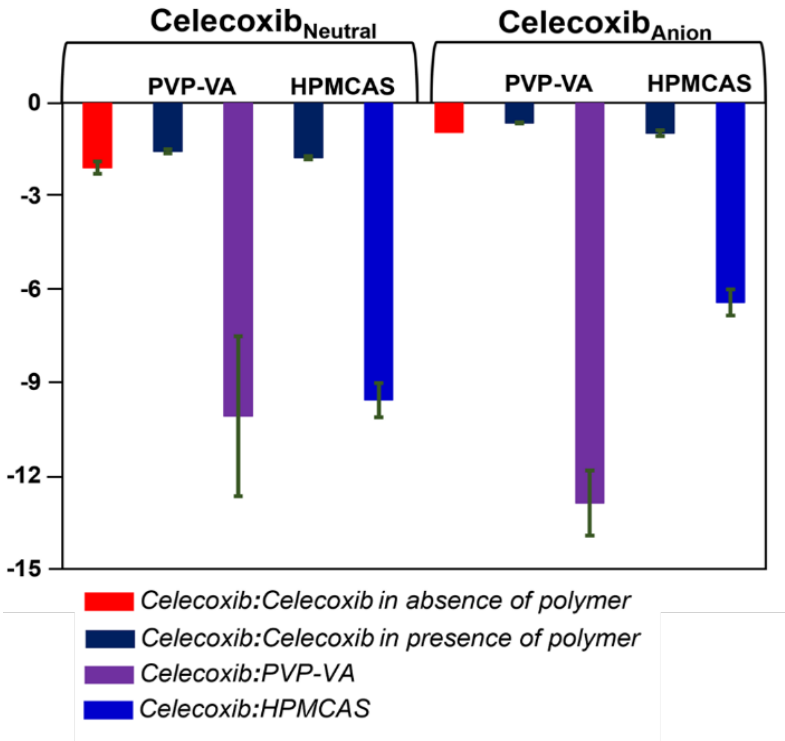

1310 **Fig. 5. Computational analysis of the drug-polymer systems to predict suitable**
1311 **polymer excipients.** Computed MM/GBSA energies (kcal/mol) for the CEL:CEL
1312 (red, deep blue),CEL:PVP-VA (purple) and CEL:HPMCAS (blue) interactions
1313 show the more energetically favorable interactions of PVP-VA with CEL than
1314 HPMCAS, particularly for the anionic form of CEL. The averages and standard
1315 deviations of the energies computed from the two replica simulations for each
1316 system are shown. Computed values are given in Table S1 and their decomposition
1317 is given in Table S2.

1318
1319

1320

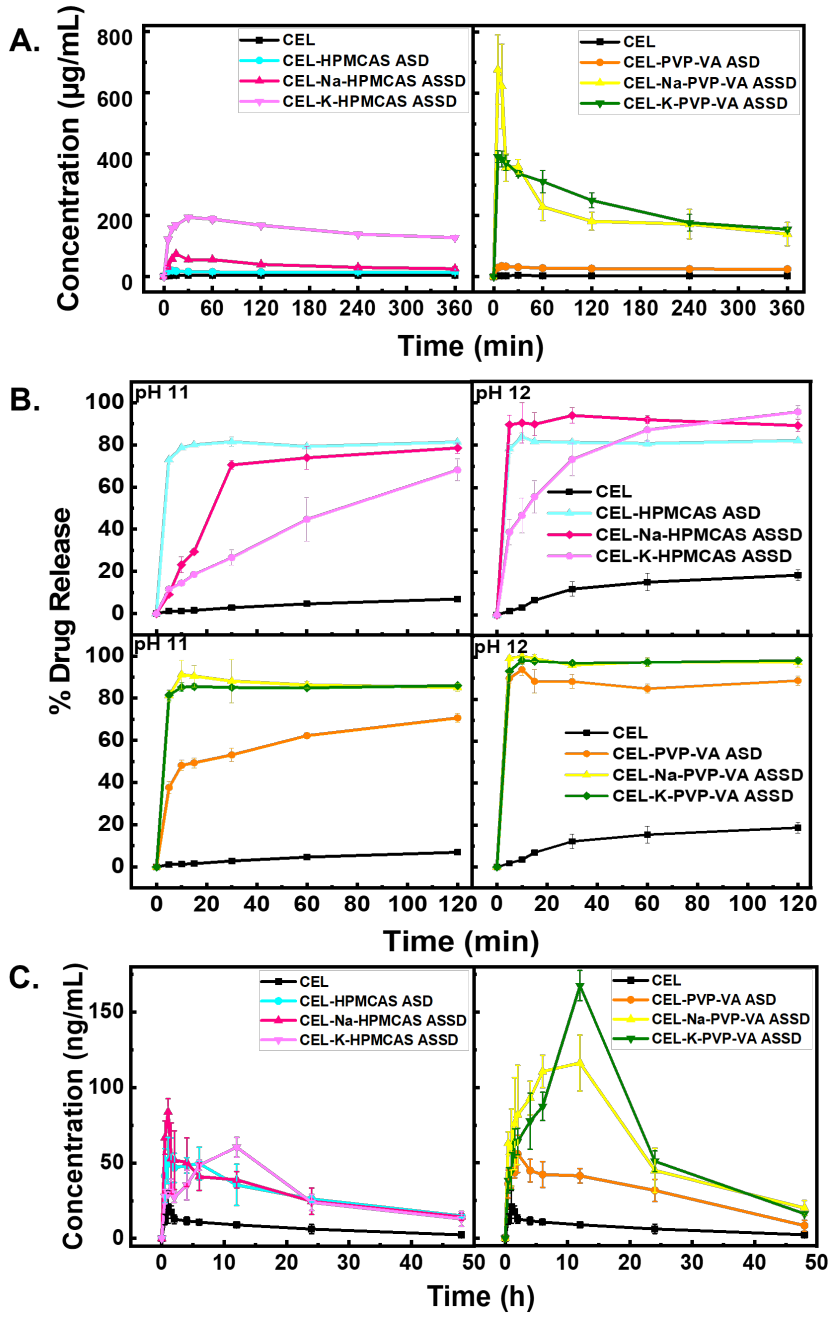

1321 **Fig. 6. Biopharmaceutical properties of crystalline CEL and its amorphous**
1322 **formulations. (A)** Apparent solubility in aqueous medium (water) for 6 h. **(B)**
1323 Dissolution profile under sink and non-sink conditions in pH 11 and 12 buffer
1324 media, respectively, for 2 h as per OGD recommendation for dissolution
1325 performance. Measurements for (A) and (B) were made in triplicate. **(C)** Plasma
1326 concentration vs time profile from pharmacokinetic studies performed for 48 h in
1327 SD female rats (n=5; data provided in accompanying Excel file).

1328
1329

1330 **Table 1. Solubility parameter values calculated by the Fedors and HVK methods for**
1331 **CEL and the two polymers studied.**

Name of compound	**Fedors method: Hildebrand solubility parameter δ ($MPa^{1/2}$)**	**HVK method: Hansen solubility parameter δ ($MPa^{1/2}$)**	**Mean δ ($MPa^{1/2}$)**	**Δδ ($MPa^{1/2}$) (δ_{drug}-$\delta_{polymer}$)**	**Flory–Huggins (F-H) interaction parameter χ (drug-polymer)**
Celecoxib	23.88	23.82	23.85	--	--
PVP-VA	22.74	22.94	22.84	1.01	0.100
HPMCAS	22.40	24.00	23.20	0.65	0.041

1332
1333

1334 **Table 2. Specifications of the systems simulated to study the aggregation of CEL.** MD
1335 simulations were carried out for polymeric excipients without CEL (a,b), and for
1336 the neutral (c,d,g,i) and anionic (e,f,h,j) forms of CEL in the absence (c-f) and
1337 presence (g-j) of a polymeric excipient. The periodic box extent, the numbers of
1338 TIP3P water molecules, Na^+ and Cl^- ions, and the simulation time are given for
1339 each simulation system. Each drug-polymer system was simulated in duplicate,
1340 generating trajectories referred to as replica-1 and replica-2. For the systems
1341 without polymer, two systems with different initial box sizes were each simulated
1342 once, generating only a replica-1 trajectory.

System	# and ionization state of CEL	Polymer and its length (Å)	Box size (Å)*	# of water molecules	# of Na^+	# of Cl^-	Simulation length (ns)
a	0	PVP-VA (75.1)	X=154.2; Y= 94.3; Z= 99.9	46569	0	0	66
b	0	HPMCAS (79.2)	X =158.2; Y = 127.3; Z = 99.2	58720	4	0	66
c	13 neutral	---	112	138672	9	9	516
d	11 neutral	---	106	117072	7	7	456
e	13 anionic	---	112	138672	22	9	916
f	11 anionic	---	106	117066	18	7	1042
g	13 neutral	PVP-VA (43.9)	112	46031	9	9	356
h	13 anionic	PVP-VA (43.9)	112	46038	22	9	356
i	11 neutral	HPMCAS (72.2)	106	38819	11	7	376
j	11 anionic	HPMCAS (72.2)	106	38831	22	7	376

1343 *The initial box was cubic unless specified by giving the X, Y and Z dimensions.
1344

1345 **Table 3. *In vivo* pharmacokinetic parameters of crystalline CEL, and CEL ASD and ASSD**
1346 **formulations.**

Formulations	C_{max} (ng/mL)	Fold increase	T_{max} (h)	AUC (ng.h/mL)[#]	Fold increase	MRT (h)	$T_{1/2}$ (h)
Crystalline CEL	20.94± 10.85	-	1± 0.28	374.09± 25.98	-	24.09± 2.35	17.5± 1.45
CEL-PVP-VA ASD	55.93± 12.21	2.67	2± 0.5	1632.67± 226.76	1.79	23.44± 3.45	15.14± 3.20
CEL-Na-PVP-VA ASSD	116.23± 18.45*	5.55	12± 0.0	3327.57± 151.68	8.89	22.56± 0.54	14.89± 0.36
CEL-K-PVP-VA ASSD	167.47± 10.02*	7.99	12± 0.0	3519.76± 124.77	9.40	19.26± 0.19	11.12± 0.09
CEL-HPMCAS ASD	51.66± 15.28	2.46	1± 1.73	1615.63± 126.54	4.36	27.18± 3.89	19.11± 3.41
CEL-Na-HPMCAS ASSD	83.89± 8.74	4.00	1± 0.28	1878.63± 101.56	5.02	34.49± 0.98	24.41± 0.85
CEL-K-HPMCAS ASSD	60.49± 6.52	2.88	12± 0.0	1774.5± 192.29	4.74	26.8± 2.86	17.25± 2.36

1347 *$p < 0.05$, statistically significant difference in comparison with crystalline CEL at n=3 (n=
1348 no of animals in each group)

1349 [#]The fold increase represents the fold-enhancement in the C_{max} and AUC of prepared
1350 formulations compared to pure crystalline CEL.

1351
1352